NASA/CR—2006-214085

Two Phase Flow Modeling: Summary of Flow Regimes and Pressure Drop Correlations in Reduced and Partial Gravity

R. Balasubramaniam, E. Ramé, J. Kizito, and M. Kassemi
National Center for Space Exploration Research, Cleveland, Ohio

January 2006

The NASA STI Program Office . . . in Profile

Since its founding, NASA has been dedicated to the advancement of aeronautics and space science. The NASA Scientific and Technical Information (STI) Program Office plays a key part in helping NASA maintain this important role.

The NASA STI Program Office is operated by Langley Research Center, the Lead Center for NASA's scientific and technical information. The NASA STI Program Office provides access to the NASA STI Database, the largest collection of aeronautical and space science STI in the world. The Program Office is also NASA's institutional mechanism for disseminating the results of its research and development activities. These results are published by NASA in the NASA STI Report Series, which includes the following report types:

- TECHNICAL PUBLICATION. Reports of completed research or a major significant phase of research that present the results of NASA programs and include extensive data or theoretical analysis. Includes compilations of significant scientific and technical data and information deemed to be of continuing reference value. NASA's counterpart of peer-reviewed formal professional papers but has less stringent limitations on manuscript length and extent of graphic presentations.

- TECHNICAL MEMORANDUM. Scientific and technical findings that are preliminary or of specialized interest, e.g., quick release reports, working papers, and bibliographies that contain minimal annotation. Does not contain extensive analysis.

- CONTRACTOR REPORT. Scientific and technical findings by NASA-sponsored contractors and grantees.

- CONFERENCE PUBLICATION. Collected papers from scientific and technical conferences, symposia, seminars, or other meetings sponsored or cosponsored by NASA.

- SPECIAL PUBLICATION. Scientific, technical, or historical information from NASA programs, projects, and missions, often concerned with subjects having substantial public interest.

- TECHNICAL TRANSLATION. English-language translations of foreign scientific and technical material pertinent to NASA's mission.

Specialized services that complement the STI Program Office's diverse offerings include creating custom thesauri, building customized databases, organizing and publishing research results . . . even providing videos.

For more information about the NASA STI Program Office, see the following:

- Access the NASA STI Program Home Page at ***http://www.sti.nasa.gov***

- E-mail your question via the Internet to help@sti.nasa.gov

- Fax your question to the NASA Access Help Desk at 301–621–0134

- Telephone the NASA Access Help Desk at 301–621–0390

- Write to:
  NASA Access Help Desk
  NASA Center for AeroSpace Information
  7121 Standard Drive
  Hanover, MD 21076

NASA/CR—2006-214085

Two Phase Flow Modeling: Summary of Flow Regimes and Pressure Drop Correlations in Reduced and Partial Gravity

R. Balasubramaniam, E. Ramé, J. Kizito, and M. Kassemi
National Center for Space Exploration Research, Cleveland, Ohio

Prepared under Cooperative Agreement NCC3–975

National Aeronautics and
Space Administration

Glenn Research Center

January 2006

Available from

NASA Center for Aerospace Information
7121 Standard Drive
Hanover, MD 21076

National Technical Information Service
5285 Port Royal Road
Springfield, VA 22100

Available electronically at http://gltrs.grc.nasa.gov

EXECUTIVE SUMMARY

The purpose of this report is to provide a summary of state-of-the-art predictions for two-phase flows relevant to Advanced Life Support. The main focus is to identify gaps in predictive capabilities in partial gravity. The motivation is that the long duration missions being considered cannot afford to carry all the needed water for the trip. Consequently, recycling processes for water and other life support resources must be used. The operation of these processes must be validated for the relevant gravity conditions (e.g., zero for the trip, and the planetary gravity for the length of the stay there). Naturally, this is not a comprehensive review. We strive to pick out the most used and accepted models for pressure drop and flow regime prediction. As expected, there is a great history of work that applies to terrestrial conditions. More recently, a good number of works (but very small compared to those for terrestrial gravity) have addressed two-phase flows in microgravity conditions. A gap is evident in the lack of information on how to predict flows in partial gravity, especially for Lunar and Martian applications. Filling this knowledge gap will be the basis for the recommendations for future work that we will develop following this report.

After a summary of flow regimes and pressure drop correlations for terrestrial and zero gravity, we analyze the fully developed annular gas-liquid flow in a straight cylindrical tube. This flow is amenable to analytical closed form solutions for the flow field and heat transfer. In this flow, the gas flows in the center and the liquid forms an annulus next to the tube wall. No gas bubbles are present in the liquid, nor liquid drops in the gas. In this respect, our analysis differs from real annular flows where typically liquid droplets are entrained by the gas core. Therefore, these solutions may be used as baselines and guides to which realistic measurements in similar flows may be compared. We have also attached in an appendix the material we submitted in a previous short report concerning the flow regimes likely to be encountered in the water recovery equipment currently under consideration for space applications. The report is a follow-up on recommendation developed in the workshop by Chiaramonte and Joshi, 2004 where issues relevant to (i) air revitalization (ii) water recovery and (iii) thermal systems, particularly of interest to the Advanced Life Support were discussed.

Table of Contents

Nomenclature

α	denotes the thermal diffusivity m^2/s
β	thermal conductivity ratio
Δp	Pressure drop along the pipe N/m^2
$\dot{m}$	total rate of mass flow per unit area in the pipe Kg/s
ϵ_{GA}	area averaged local void fraction of the gas
μ_G	gas viscosity $N.s/m^2$
μ_H	effective viscosity $N.s/m^2$
μ_L	liquid viscosity $N.s/m^2$
ϕ	angle between the vertical the flow direction
ρ_H	effective density Kg/m^3
ρ_{eff}	effective density kg/m^3
ρ_G	gas density Kg/m^3
ρ_L	liquid density Kg/m^3
σ	Surface Tension N/m
τ_W	wall shear stress N/m^2
θ	contact angle of the liquid-gas interface at the solid
$\tilde{h}$	heat transfer coefficient $W/m^2.K$
Bo	static Bond number
c_{p_G}	gas heat capacity $J/kg.K$
c_{p_L}	liquid heat capacity $J/kg.K$
Ca	Capillary Number
D	pipe diameter m
F	gravitational parameter
f_{ent}	fraction of liquid drops entrained
Fr	modified Froude number
g	gravitational acceleration m/s^2
g_z	component of gravity along the axis of the tube m/s^2

H mean curvature of the interface $1/m$

h constant gas core thickness m

Int_{Gas} Integral of the gas core in eq. 40

Int_{Liq} Integral of the liquid in eq. 40

k_L liquid's thermal conductivity $W/m.K$

M gas to liquid viscosity ratio

Nu Nusselt number

P'_G physical pressure in the gas phase N/m^2

P'_L physical pressure in the liquid phase N/m^2

Pe Péclet number

q^* constant heat flux per unit wall area W/m^2

Q_{Gf} gas volume flow fraction

Q_G liquid flow rates m^3/s

q_{LD} liquid flow rate that is flowing as drops m^3/s

Q_{LF} liquid flow rates m^3/s

Q_L liquid flow rates m^3/s

R radius of pipe m

Re_G gas Reynolds number

Re_L liquid Reynolds number

S Slip ratio

Su Suratman number $\equiv Re/Ca = Re^2/We$

t constant liquid film thickness m

U total superficial velocity m/s

U_{GS} superficial gas velocity m/s

U_{LS} superficial liquid velocity m/s

w^* axial velocity field m/s

We Weber number

x quality (the gas mass flow fraction)

X^2 ratio of liquid-to-gas frictional pressure gradients with each phase flowing alone in the pipe

1 Introduction to two-phase flow

Two-phase flows involving liquids and gases regularly occur in advanced life support systems operating in space environments. These flows cannot be avoided; therefore there is a need to understand how these flows can potentially affect the performance and longevity of life support hardware. Two-phase flows are critical to regenerative life support technologies, specifically water and atmosphere management. In these flows, the pressure drop and the rates of transfer of heat and mass are strongly influenced by the flow regimes which in turn are controlled by the relative flow rates and the dimensions of the component carrying the fluid mixture.

The ultimate goal of this project is to develop predictive analytical and computational tools for two-phase flow with and without phase change in low and partial-g environments, for applications to Advanced Life Support. The tools will be applicable not only for design but also for predicting performance of space systems from ground-based test data.

Two-phase flow of gas and liquid, and multiphase flow of gas, liquid and solid have been identified and given high priority in the final report of a workshop on critical issues in microgravity fluids, transport and reaction processes (Chiaramonte and Joshi, 2004 [4]). This workshop developed several important recommendations for research in applications to Advanced Life Support.

In this report we have reviewed and cataloged adiabatic two-phase flow behavior in a pipe. Predictions for the flow regime in normal and reduced gravity, and available correlations for the pressure drop and rate of heat transfer are summarized. To write this report we have have used information from published knowledge, analysis of basic equations that describe flow and information gathered from technical reports by ETH 2005 [5] and Lahey *et al.* 2003 [6].

1.1 Background

Multiphase technology is likely to become necessary in regenerative life support systems in missions to the Moon or Mars because it will not be possible to carry from Earth all the resources needed for the trip. Similarly, heat exchange with phase change will be a must because of its superior efficiency-to-volume ratio. Unfortunately, two-phase technologies have not yet been widely implemented in space due to lack of reliability from poor prediction tools in non-terrestrial gravity environments. Nevertheless, two phase flow is often encountered is several space systems that are planned to be used (Eckart, 1996). Examples of some specific systems are: Vapor Phase Catalytic Ammonia Removal (VPCAR), Vapor Compression Distillation VCD), Thermoelectric Integrated Membrane Evaporation System (TIMES), Electrolysis Plant (ELEKTRON), Supercritical Water Oxidation (SCWO) and Condensing Heat Exchanger (CHX). These space systems are used for revitalization of air in the spacecraft and in the recovery and recycling of water. Some information on the rates of flow of air and water in these systems and the regimes of two phase flow that occur are summarized in Appendix D.

The workshop by Chiaramonte and Joshi, 2004 [4] developed several important recommendations for research in applications to (i) air revitalization (ii) water recovery (iii) solid waste management and (iv) thermal and phase change systems. We summarize below the applications of multiphase flow identified by this workshop in each of these categories.

Water recovery systems provide a safe supply of potable water critical for human life for long-term space flight. Resupply is unlikely in long-term flight, and the recovery and use of wastewater is necessary. The workshop report states that multiphase flow is currently avoided in the design of waste water recovery systems, and that being able to use multiphase flow systems under microgravity could permit the use of technologies for water recovery that have not been considered before. The understanding of multiphase flow and separation in microgravity was identified as a critical, high priority need for design of water recovery systems.

Thermal and phase change systems require enabling technologies for efficient and reliable generation, storage and transfer of energy. Currently, most of the subsystems involve single-phase fluid and thermal processes. Future subsystems such as boilers, condensers, evaporators, heat exchangers, fuel cells, heat pipes, etc., will involve multiphase flow so that the energy-to-mass ratios are improved. The following areas for research in microgravity, among several others, have been identified as having high priority with critical and severely limiting issues in the workshop report: phenomenological understanding for multi-phase flow in micro and macro geometries; boiling, condensation, phase distribution and phase transition; development of empirical correlations, theoretical models, scaling laws and CFD codes for two-phase flow in complicated geometries; stability criteria for two-phase flow loops; development of advanced technologies for phase separation.

Air revitalization systems are used for environment conditioning and life support (ECLS) for the crew. They are necessary for survival of the crew (such as oxygen supply and carbon dioxide removal) and to maintain crew health and safety (such as fire detection and suppression, humidity control, and detection and removal of particulate matter and trace contaminants in air). Control of particulate matter in the air stream, separation of gases from liquids, and degassing of liquids is a common thread in many of the systems utilized for air revitalization. The workshop report recommends continued effort to understand and develop techniques for phase separation and liquid degassing. More importantly, it determined that key information useful for designing ECLS systems is not available in a format readily useful to designers, but is scattered in the literature on microgravity research, and in commercial aerospace and academic communities. Compiling the existing information into design guides detailing the mechanisms, behaviors, fundamentals and the relevant physics, as well as providing scaling analysis, correlations, summary of flight experiment data into a usable format for the ECLS design community was given a high priority.

1.2 Description of two phase flow

In two phase flow, two phases, typically gas and liquid flow through a system, such as a pipe, simultaneously. Because the liquid/gas interface can deform, the location of the regions occupied by gas and liquid in the pipe is unknown to begin with and is of great interest in designing the two phase flow system. Some of the common states of the two phases are: (i) *bubbly flow*, in which the gas is present within the liquid in the form of innumerable bubbles of small size (ii) *slug flow* where individual gas bubbles merge to form a large gas mass or slug that is often cylindrical in shape (iii) *stratified flow* where the gas and liquid regions are separated, with the gas that is lighter flowing on top of the heavier liquid (iv) *annular flow* where one fluid (typically the liquid) occupies the space adjacent to the tube wall and surrounds the other fluid (gas) that flows in the center of the tube. Where the liquid is, where the gas is, and in what form, is determined from a flow regime map. Such a map attempts to connect the observations made of the state of the two phase flow to the tube size, physical properties of the liquids, and the rates at which the liquid and gas flow. The liquid and gas flow rates are often specified in terms of superficial velocities, which is the velocity of the liquid or gas if it alone flows through the pipe. The void fraction refers to the fraction of the space occupied by the gas in a region within the pipe. Especially of interest to the designer is the pressure drop as the two phases flow through the pipe, and in the case of non-isothermal systems, the rate at which heat can be transported in the pipe by the two phase flow.

Gravity is a crucial parameter in two phase flow. The buoyancy force exerted due of the difference in density between the gas and the liquid has a major impact on the flow regime, the distribution of void fraction, the pressure drop and the rate of heat transfer in the pipe.

1.3 Current knowledge base for reduced gravity

The purpose of this section is to review published work on two-phase flow in partial and microgravity since the pioneering work of Dukler *et al.* 1988 [7] where models are proposed to describe gas-liquid flow regimes and their transitions in microgravity conditions. These models use void fraction as a criterion describing the transition between flow regimes..

1.3.1 Background on flow regime

Zhao *et al.* 2004 [8] report a study of experimental data of two-phase flow regimes and their transitions in a 90-degree bend with inner diameter of 12.7 mm and curvature radius of 76.5 mm in microgravity conditions. In their study, the superficial gas velocities range from 1.0 to 23.6 m/s and superficial liquid velocities range from 0.09 to 0.5 m/s. The study observes three major flow regimes: slug, slug-annular transitional, and annular flows.

Takamasa *et al.* 2004 [9] measured void fraction, interfacial area concentration, bubble

Sauter mean diameter, [1] and bubble number density in bubbly flow in microgravity and low liquid Reynolds number conditions. These experiments are consistent with the flow regime map described by Jayawardena *et al.* 1997 [1]. Nonaka *et al.* 2002 [10] obtained data on two-phase flow using the drop-shafts of Hokkaido National Industrial Research Institute (HNIRI), Microgravity Laboratory of Japan (MGLAB) and Japan Microgravity Center (JAMIC). Their data show that when the length of an annular liquid film in a circular pipe exceeds a critical length under zero gravity, the liquid film breaks into periodic lobes which result into plugs. The group surmises that linear stability theory can explain the periodicity observed in the experimental data.

Choi *et al.* 2003 [11] have obtained data of flow regimes, void fraction, frictional pressure drop in normal gravity, microgravity and hyper-gravity (2g) aboard the MU-300 aircraft. They conclude that the gravity dependency of flow regimes was more clearly seen as gas and liquid flow rates decrease. The effect of gravity on two-phase flow was insignificant for the turbulent flow regions.

Zhao *et al.* 2001 [12] have performed experimental studies for horizontal two-phase air-water flows in normal and reduced gravity conditions in a square cross-section channel aboard the Russian IL-76 reduced gravity airplane. They observe four flow regimes: bubbly, slug, slug-annular transition and annular flows. In that same year, Zhao *et al.* Nov. 2001 [13] report a series of experiments performed aboard the Mir Space Station on two-phase gas-liquid flow regimes in a test tube with a length of 356 mm and an inside diameter of 10 mm. The working fluids were carbogal and air which resulted in five types of flow regimes: dispersed bubbly, bubbly, slug, slug-annular transitional, and annular. Earlier, Zhao *et al.* May 2001, [14] claim to have discovered a new region of annular flow with lower liquid superficial velocity. Previously, Zhao *et al.* 2000 [15] had developed a model for predicting the transition from slug to annular flow of adiabatic two-phase gas-liquid flow in microgravity.

Wölk *et al.* 2001 [16] describe a flow regime map for microgravity based on five dimensionless parameters. Observed regimes include: dispersed bubble, slug, slug/annular, frothy slug/annular and annular flows.

Lowe *et al.* 1999 [17] identify two-phase flow regimes in microgravity using void fraction signals on board the NASA DC-9 microgravity aircraft.

Ungar *et al.* 1998 [18] argue based on analysis of dimensionless parameters that it should be possible to simulate microgravity conditions on Earth using systems similitude. It is not clear from this work whether microgravity flow regime maps can be obtained on Earth under wholly similar conditions.

Colin *et al.* 1996 [19] suggest that the transition from bubbly to slug flow may be predicted by introducing a critical void fraction that depends on the fluid properties

[1] The Sauter mean diameter is the volume to surface area mean diameter of a distribution of bubbles.

and the pipe diameter. However, the role of coalescence which controls this transition is not clearly understood. Reinarts *et al.* 1991 [20] present data that indicates that flow regimes observed under microgravity conditions are primarily annular and include slug and bubbly-slug regimes.

1.3.2 Background on Pressure Drop

Wang *et al.* 2004 [21] present data on the interfacial friction factor and relative interfacial roughness on the gas-liquid interface for an air-water annular flow in a tube with inner diameter of 9.525 mm.[2] Their results show that while the roughness in microgravity is less than half of that in normal gravity, the friction factor was only about 10% smaller in microgravity than that in normal gravity.

Motil *et al.* 2003 [22] report experimental data on flow regime transitions, pressure drop, and flow characteristics for co-current gas-liquid flow through packed columns in microgravity. They find that two non-dimensional numbers, liquid Reynolds number and Suratman number, are important in describing flow in a packed bed in microgravity. The flow conditions in the inlet and outlet pipes can be used to determine the pressure drop across these sections. Earlier, Bousman *et al.* 1996 [23] presented data on two-phase gas-liquid flow in the reduced gravity aircraft for void fraction, liquid film thickness and pressure drop.

Takamasa *et al.* 2003 [24] present data which they claim can be used for the development of reliable constitutive relations which reflect the true transfer mechanisms in two-phase flow in microgravity. These relations can be used to determine the pressure drop across the pipe section. They measure bubble number density, interfacial area concentration, and Sauter mean diameter of adiabatic nitrogen-water bubbly flows in a 9-mm diameter pipe using image processing.

Kamp *et al.* 2001 [25] developed a mechanistic model for bubble coalescence in turbulent flow. Their model can be used to predict pressure drop in pipes. Their model was validated by data obtained in a reduced gravity aircraft. They conclude that, in the absence of gravity, collisions between bubbles smaller than the length scale of turbulence are primarily due to turbulence.

Iguchi *et al.* 2001 [26] report wettability of the pipe did not affect the mean rising velocity of bubbles in microgravity. Taitel *et al.* 1996 [27] present a model to predict slug flow in microgravity. Colin *et al.* 1995 [28] report experiments on gas-liquid flow in small tubes of 19 mm, 10 mm and 6 mm diameter obtained during reduced gravity flights, for a range of superficial liquid velocities from 0.1 to 2 m/s and superficial gas velocities from 0.05 m/s to 10 m/s. Their results show how coalescence and the wall friction factor affect pressure drop. Also, Zhao *et al.* 1995 [29] provide experimental data on pressure drop of air-water two-phase flow in microgravity obtained aboard the NASA KC-135 aircraft. They compare pressure drop data between μ-g and 1-g vertical flows. They indicate that the magnitude of pressure drop in both cases is similar.

[2]The interfacial friction factor, f_i, relates to the drag at the liquid-gas interface in the same way the conventional friction factor applies to the drag at the solid-fluid interface.

Zhao *et al.* 1993 [30] present data on two-phase air-water flow pattern data obtained aboard NASA KC-135 aircraft. The liquid superficial velocity ranges from 0.09 to 3.73 m/s, and the gas superficial velocity from 0.2 to 29.9 m/s. In this parameter range they observe bubbly, slug, frothy slug-annular and annular flows. In the same year, Wheeler *et al.* 1993 [31] present a comparison between two-phase flow and single phase systems for space applications. The advantages include capability of achieving high specific power levels. They performed experiments on a reduced gravity aircraft where annular flow pressure drops were measured through 10.41-mm ID 1.251-m long glass tubing during periods with acceleration levels in the range 0.05 g. They conclude that the reduced acceleration interfacial friction factor data was not predicted by the 1-g models.

1.3.3 Background on Heat Transfer

Colin 2002 [32] has raised some important questions regarding two-phase flow in microgravity. These issues are motivated by the technical problems arising in the design of thermo-hydraulic loops for space applications. Further, she states that most of the studies are focused on the determination of the flow regime, wall shear stress, heat transfer and phase fraction. These data have led to many empirical correlations without a clear understanding of some of the basic mechanisms involved. Colin illustrates this point with an example showing that the transition from bubbly to slug flow is well predicted by a critical value of the void fraction depending on the Ohnesorge number ($Oh \equiv Su^{-1/2}$, see section 2.1). One limitation is that the transition criterion does not take into account the pipe length and the bubble size at the pipe inlet. In most cases, to improve this criterion, a physical model of bubble coalescence in turbulent flow is used to predict the bubble size evolution along the pipe in microgravity. Another issue concerns the radial distribution of bubbles in pipe flow which is very sensitive to gravity and affects heat transfer.

Fore *et al.* 1997 [33] present measurements on both fluid flow and heat transfer for two-phase slug flows in microgravity. They use air and two liquids (water and a 50% aqueous glycerine solution) to obtain a range of liquid Reynolds numbers from 1000 to 20,000 in a 25.4 mm inner diameter tube. They show based on a comparison of microgravity to normal-gravity correlations that the heat transfer coefficients are smaller in reduced-gravity than in normal-gravity under the same flow conditions. They surmise that smaller liquid-phase turbulence levels in the absence of buoyancy-induced slip between the gas and liquid can explain this difference.

1.3.4 Background on Computational Modeling

In this report, we do not consider the computational modeling of two-phase flow, except for the brief introduction to the subject given below. There have been several studies on the computational modeling of two-phase flow, mostly in normal gravity. The most popular approach is the multi-field two-fluid model (Lahey, 2002 [6]), and appears to be the state of the art. In particular, a four-field two-fluid model appears to be capable of describing the features of different flow regimes in normal gravity. In

what follows, we briefly summarize this approach. The four fields comprise of continuous vapor, continuous liquid, dispersed vapor and dispersed liquid. The unknowns in this model at a point in the computational domain are (i) the volume fraction of each of the fields (ii) the velocity vector of these fields (iii) the pressure of each field (iv) the enthalpy of each field. For each field, equations representing the ensemble average of conservation of mass, momentum and energy are written. Source and sink terms are present in these equations to represent the inter-conversions of these quantities among the fields. In order to achieve closure of the system of equations and unknowns, jump conditions for momentum and energy transport across the interface of a pair of the fields are written. For bubbly flow, this would involve the jump momentum and energy balances across the interfaces between a continuous liquid and dispersed vapor phases. Empirical laws using drag coefficients are used for the contribution to the momentum balance arising from drag forces. Typically, the interfacial area density appears in these empirical laws. An interfacial area transport equation is usually obtained using kinetic theory methods. Where necessary, potential flow theory is also used to derive many of the interfacial transfer laws. Appropriate models for turbulence are incorporated in the conservation equations and interfacial transfer laws.

The results from such simulations for the void fraction distribution and liquid velocity profile are reported to be in good agreement with experiments for up-flow and down-flow of air and water. The readers should consult Lahey (2002) [6] for more details and further examples illustrating the use of four-field two-fluid model, such as pressure drop, prediction of transient phenomena, etc.

Several researchers have used direct numerical simulations to model multi-phase flows. Some of the approaches used are volume of fluid (VOF) methods [34], level set methods, sharp interface methods and phase field methods [34], and embedded interface methods [34].

Most of the four-field two-fluid modeling studies as well as the direct numerical simulations appear to have been conducted for two-phase flow under normal gravity, but in principle they are applicable for modeling flows in microgravity and partial gravity.

2 Dimensionless parameters in two-phase flow

We will consider two-phase flow phenomena when the two phases are being transported via a pipe or a channel from one reservoir to another. In what follows we only deal with isothermal flow of gas and liquid. A knowledge of the dimensionless parameters in two phase flow is useful because, as in single phase flow, it can enable theoretical and experimental results for a particular flow situation (fluids, tube size, velocities, gravity level etc.) to be scaled and extrapolated to a different flow situation. Quite often, casting results in terms of dimensionless parameters can also provide a clue to the underlying physical mechanisms.

2.1 Use of the Buckingham Pi Theorem

The independent variables are:

$$U_{LS},\ U_{GS},\ \mu_L,\ \mu_G,\ \rho_L,\ \rho_G,\ D,\ \sigma,\ g \text{ and } \phi. \tag{1}$$

These symbols denote the superficial liquid velocity, superficial gas velocity, liquid viscosity, gas viscosity, liquid density, gas density, pipe diameter, surface tension, gravitational acceleration, and angle between the vertical and the flow direction. The superficial velocity is the average velocity each phase would have if it alone flows in the pipe. There are ten variables and three fundamental units (mass, length and time). Using the Buckingham Pi theorem, this yields seven independent dimensionless parameters. One set of dimensionless parameters is:

$$\begin{aligned} Re_L = \frac{\rho_L U_{LS} D}{\mu_L},\ Re_G = \frac{\rho_G U_{GS} D}{\mu_G},\ Fr_L = \frac{\Delta\rho}{\rho_L}\frac{gD}{U_{LS}^2}, \\ We_L = \frac{\rho_L U_{LS}^2 D}{\sigma},\ \frac{\mu_G}{\mu_L},\ \frac{\rho_G}{\rho_L},\ \phi \end{aligned} \tag{2}$$

where Re_L is the liquid Reynolds number, Re_G is the gas Reynolds number, Fr_L is a modified Froude number in the liquid, We_L is the Weber number in the liquid and $\Delta\rho \equiv \rho_L - \rho_G$. A commonly used parameter is the slip ratio defined as:

$$S = \frac{U_{GS}}{U_{LS}} \tag{3}$$

may be derived from the liquid and gas Reynolds numbers and the viscosity ratio. Other dimensionless parameters derivable from the above set are the Suratman number:

$$Su = \frac{Re_L^2}{We_L} = \frac{\rho_L D\sigma}{\mu_L^2} \tag{4}$$

that has been used in the literature and is important in demarcation of flow regime transition boundaries in low gravity, and the static Bond number:

$$Bo = \frac{(\rho_L - \rho_G) g D^2}{\sigma} \tag{5}$$

which is the ratio of the buoyancy to surface tension forces. A question arises as to what the natural set of seven dimensionless parameters is. To determine these, we perform a scaling analysis of the governing equations for two phase flow in the absence of heat transfer.

2.2 Scaling Analysis of Two Phase Flow

The governing equations for two phase flow that we consider are the incompressible Navier-Stokes equations. They are written separately for the liquid and gas phase below.

$$\rho_L \left(\frac{\partial \mathbf{U}_L}{\partial t} + \mathbf{U}_L \cdot \nabla \mathbf{U}_L \right) = -\nabla P_L + \mu_L \nabla^2 \mathbf{U}_L \tag{6}$$

$$\rho_G \left(\frac{\partial \mathbf{U}_G}{\partial t} + \mathbf{U}_G \cdot \nabla \mathbf{U}_G \right) = -\nabla P_G + \mu_G \nabla^2 \mathbf{U}_G - (\rho_L - \rho_G)\mathbf{g} \tag{7}$$

where $\nabla P_L = -\rho_L \mathbf{g} + \nabla p_L^*$, $\nabla P_G = -\rho_L \mathbf{g} + \nabla p_G^*$, $\nabla p_G^* - \rho_G \mathbf{g} = \nabla P_G - (\rho_L - \rho_G)\mathbf{g}$ and $p_L^*,\ p_G^*$ denote the physical pressures in the liquid and gas phases.

We choose the following reference quantities to normalize the variables.

- Gas velocity – U_{GS} = Superficial gas velocity
- Liquid velocity – U_{LS} = Superficial liquid velocity
- Time – $\frac{D}{U_L}$
- Length – D = pipe diameter
- Gas pressure – $\rho_L U_{LS}^2$
- Liquid pressure – $\rho_L U_{LS}^2$

Before we proceed we discuss the choice for the pressure normalization given above. Both the liquid and gas pressures are referred to the same datum (the hydrostatic pressure in the liquid at any z plane) and is scaled by $\rho_L U_{LS}^2$. Consider a two phase flow in which the liquid forms the continuous phase, and contains many gas bubbles as the dispersed phase. We expect the pressure within a gas bubble to be equal to the pressure in the liquid surrounding it, except for a contribution arising from surface tension. Thus the gas and liquid pressures adjacent to the liquid/gas interface are approximately the same. The normalization scheme we have chosen for the pressures

reflects this idea. If drops of liquid are present in a gas as the continuous phase, the density of the gas ρ_G and its superficial velocity U_{GS} must be used in normalizing the pressure in the liquid and gas. The pressure normalization factors in the liquid and gas can be different for stratified flow and developing or entrance flows. The scaling analysis performed here is not valid for such situations and must be suitably modified.

With these choices the governing equations can be written in the following dimensionless form.

$$\frac{\partial \mathbf{u}_L}{\partial t} + \mathbf{u}_L \cdot \nabla \mathbf{u}_L = -\nabla p_L + \frac{1}{Re_L} \nabla^2 \mathbf{u}_L \tag{8}$$

$$S\frac{\partial \mathbf{u}_G}{\partial t} + \mathbf{u}_G \cdot \nabla \mathbf{u}_G = -\nabla p_G + \frac{1}{Re_G} \nabla^2 \mathbf{u}_G - Fr_G \frac{\mathbf{g}}{|g|}, \tag{9}$$

where $Fr_G = \frac{\Delta\rho}{\rho_G} \frac{gD}{U_{GS}^2}$. We next look at the balance of shear and normal stresses at the liquid/gas interface. When the surface tension is uniform (i.e., no Marangoni stress at the interface), the balance of shear stress yields

$$\left(\frac{\mu_L U_{LS}}{\mu_G U_{GS}}\right) \frac{\partial u_L}{\partial s} = \frac{\partial u_G}{\partial s} \tag{10}$$

where s is distance tangential to the interface. The balance of normal stress may be written as

$$We_L \left(p_G - p_L\right) + 2\ Ca\ \left(\frac{\partial u_{Ln}}{\partial n} - \frac{\mu_G U_{GS}}{\mu_L U_{LS}} \frac{\partial u_{Gn}}{\partial n}\right) = 2H \tag{11}$$

where $Ca = \frac{\mu_L U_{LS}}{\sigma}$ is the Capillary number, H is the mean curvature of the interface and n is distance normal to the interface.

Thus the scaling analysis reveals that the dimensionless parameters in two phase flow are the gas and liquid Reynolds numbers, the slip ratio, the gas phase Froude number, the viscosity ratio, and the liquid phase Weber number. The orientation angle ϕ is an additional parameter which appears implicitly in the components of $\mathbf{g}$ with respect of the direction of flow. The density ratio, Capillary number and Bond number can be derived from the above dimensionless groups.

When the cross section of the flow duct is not circular, the hydraulic diameter,

$$D_h \equiv \frac{Flow\ Area}{Flow\ perimeter}$$

should be used instead of D.

2.3 Parameter Range on Current Life Support Hardware

We have performed a comparative study of the dimensionless parameters and flow regimes likely to occur in life support hardware operating in microgravity. In water

recovery equipment, the Reynolds number of gas and liquid are small to moderate. The details are shown in Appendix D. We have used the flow regime maps of Jayawardena *et al.* [1]. We have made educated assumptions about the pipe diameter where two-phase flow might arise in such hardware, and about the coexistence of water and air in that pipe. The results are flow regime predictions for typical flow rates quoted in the literature (Eckart 1996 [35], Eckart 1997 [36], Wieland 1998 [37], Wieland 1998 [38], Wieland 1994 [39]). However, we find that the Jayawardena flow map should be taken with some skepticism in predicting flow regimes in water recovery equipment. Critical analysis of the Jayawardena flow map indicates that it may apply best only when gas and liquid flow at high Reynolds numbers. Therefore, it seems prudent to undertake an experimental program to establish microgravity and partial gravity flow regime maps valid in the low-to-moderate Reynolds number flows likely to be encountered in water recovery equipment.

3 Flow Regimes in Reduced Gravity

3.1 Description of flow regimes

Jayawardena *et al.* [1] say that in the absence of gravity three major flow patterns exist – bubbly flow, slug flow and annular flow, with annular flow being obtained for a wide range of gas and liquid flow rates. For a fixed liquid flow rate, bubbly flow is obtained for low gas flow rates. This regime transitions to slug flow for higher gas flow rates. As the flow rate of the gas increases further, annular flow is obtained. For the operation of two phase flow systems, bubbly and annular flow are preferred. Because slug flow can cause vibrations, it is usually avoided. Typically, the annular flow regime yields maximum flow rates for a given two-phase system.

In bubbly flow, bubble sizes are relatively uniform, and the bubbles are distributed everywhere in the flow. Slug flow results from the merging and coalescence of individual bubbles, and the bubbles are elongated and more cylindrical in shape (Taylor bubble). The elongated gas bubbles are separated by liquid slugs. Small bubbles are often present in the liquid slugs.

In typical annular flow, the gas occupies the central or core region of the tube, with the liquid remaining in a thin layer adjacent to the tube wall. Waves are present on the liquid/gas interface and the instantaneous shape of the interface fluctuates with time. Also, small liquid drops are typically entrained by the flowing gas. Figure 1 shows pictures of bubbly, slug and annular flow obtained in low gravity.

3.2 Jayawardena *et al.*[1] reduced gravity flow regime map

In reduced gravity we can consider the value of the Froude number to be small under most circumstances, and the influence of the residual gravity on the dynamics of the two phase flow will be negligible. Therefore Fr can be omitted from the list of dimensionless parameters that influences the flow. When gravity has a negligible influence, the orientation, ϕ, of the flow relative to $\mathbf{g}$, can be omitted from the list of dimensionless parameters as well because ϕ only appears in $\rho g \sin\phi$ and $\rho g \cos\phi$. Thus, instead of the parameters Fr and ϕ, one could use $Fr_1 \equiv Fr \sin\phi$ and $Fr_2 \equiv Fr \cos\phi$. Further, the gas/liquid density and viscosity ratios typically have small values. One can therefore surmise that these two property ratios will only have a small influence on the flow. We are thus left with three dimensionless parameters – the gas and liquid Reynolds numbers and the Weber number. This is the starting point of Jayawardena *et al.* [1] in the representation of the flow regime map in terms of dimensionless parameters.

Figures 2 and 3 show the flow regime map from the work of Jayawardena *et al.* They were able to successfully capture the bubbly, slug and annular flow regimes on a single map, by plotting the Suratman number ($= \frac{\rho_L D \sigma}{\mu_L^2}$) versus the gas/liquid Reynolds number ratio or the gas Reynolds number. It is remarkable that a flow regime map for a 3-parameter system was obtained using only two dimensionless parameters (see sec. 2.3 and Appendix D for a discussion). Curiously, Motil *et al.* 2003

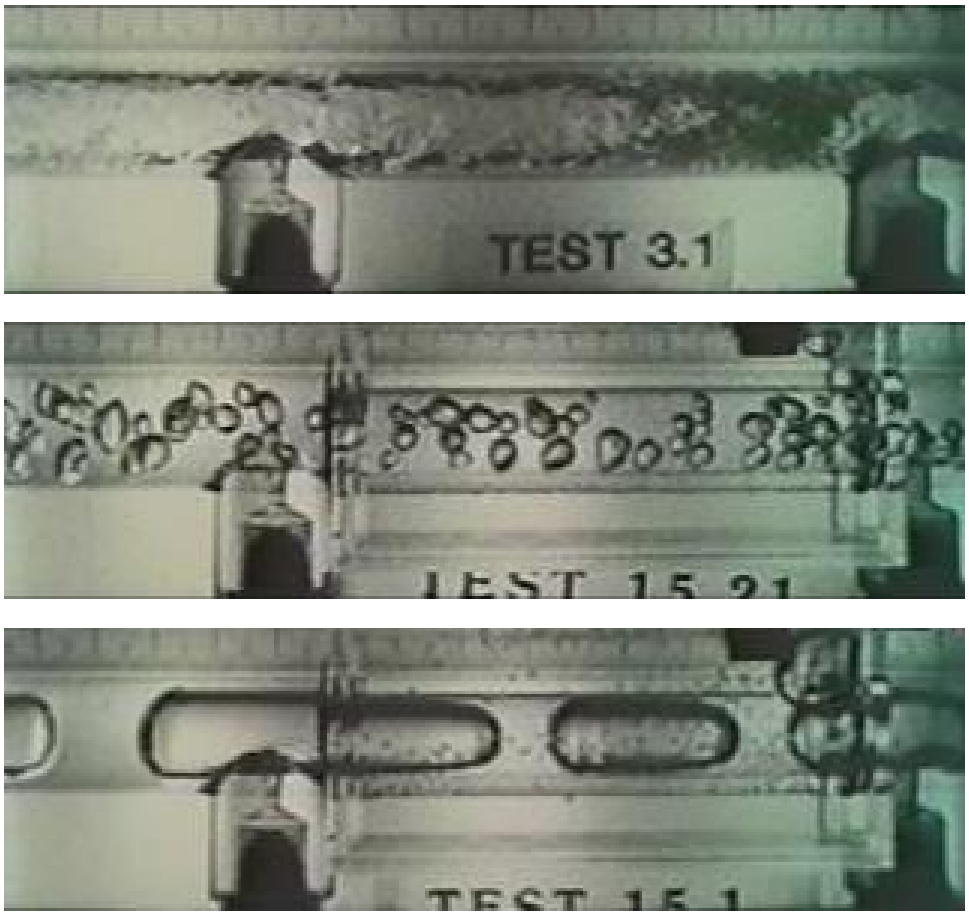

Figure 1: From top to bottom: photographs of annular, bubbly and slug flow in reduced gravity (McQuillen *et al.* [2]).

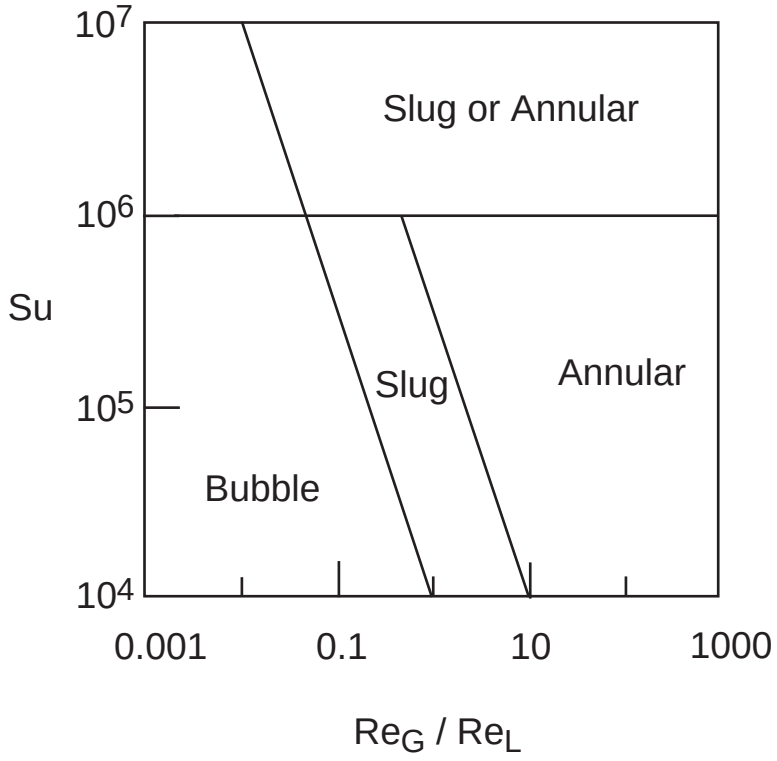

Figure 2: Flow map for zero gravity valid at $Su < 10^6$.

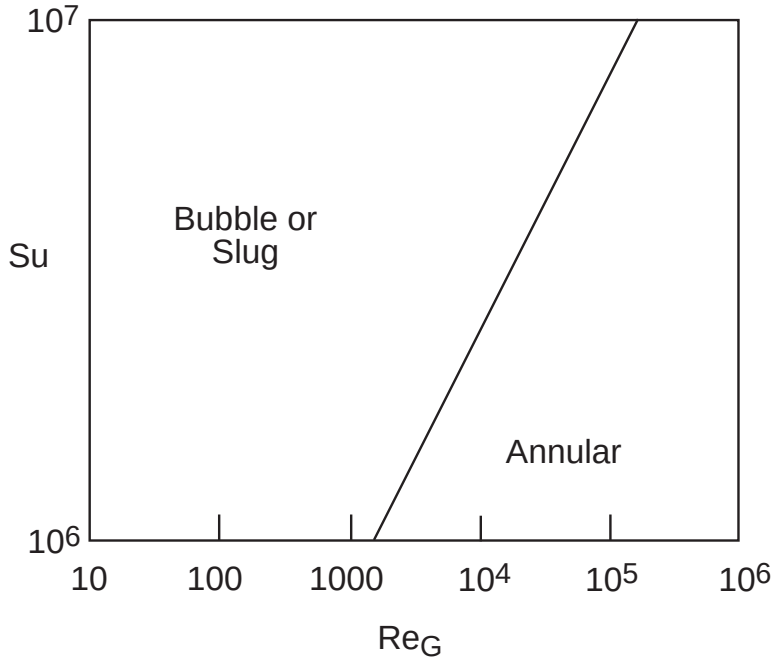

Figure 3: Flow map for zero gravity valid at $Su > 10^6$.

[22] find that a transition from bubbly flow to pulse (or slug) flow in porous, packed beds in microgravity is also captured very well on a plot of the Suratman number versus the ratio of gas to liquid Reynolds number, as in fig. 2.

3.2.1 Bubble-slug transition

Jayawardena *et al.* [1] report that the transition from bubbly flow to slug flow can be written as follows.

$$\left(\frac{Re_G}{Re_L}\right)_{transition} = 464.16\ Su^{-2/3} \tag{12}$$

It may also be written alternatively as

$$(Re_G)_{transition} = 464.16\ Ca^{2/3}\ Re_L^{1/3} \tag{13}$$

3.2.2 Slug-annular transition

Jayawardena *et al.* find that the transition from slug flow to annular flow can be written as follows.

$$\left(\frac{Re_G}{Re_L}\right)_{transition} = 4641.6\ Su^{-2/3} \qquad Su < 10^6 \tag{14}$$

$$(Re_G)_{transition} = 2 \times 10^{-9}\ Su^2 \qquad Su > 10^6 \tag{15}$$

Note that for $Su < 10^6$ the slug-annular transition occurs at a Reynolds number ratio that is a factor of 10 greater than the bubble-slug transition Reynolds number ratio. Jayawardena *et al.* [1] show that their map agrees well with nine different experiments in the open literature that used six different fluid pairs (air/water, air/water-glycerin, air/water-zonyl, R11 vapor/liquid, R12 vapor/liquid, R114 vapor/liquid) and ten different tube sizes in the range 4.7 mm to 40 mm. Specifically, the accuracy of bubble-slug transition predictions is 87%, and that for slug-annular transition is 97%.

3.3 Other flow regime transition criteria

Jayawardena *et al.*'s [1] Suratman number based flow regime map is not the only map developed for reduced gravity two-phase flow. In this section we summarize some alternative regime maps.

3.3.1 Gas void fraction criterion

Bousman's thesis [3] details the use of the Drift-flow model to estimate gas void fraction, ϵ_{GA}, knowing the superficial velocities, resulting in a relation $\epsilon_{GA} = F(U_{GS}/U_{LS})$. Since they also measured the void fraction at various flow regimes transitions, $\epsilon_{GA_{Tr}}$, they can plot the regime transition predicted from the Drift-flow model, $U_{GS} = U_{LS}\, F^{-1}(\epsilon_{GA_{Tr}})$ over the measured data. Note that the model only allows a straight line to be the flow regime boundary. The drift-flow model is adequate for predicting bubbly-to-slug transition.

Bousman also uses the drift-flow model coupled with a force balance in the annular flow to describe the slug-to-annular boundary. In this approach, expressions for the void fractions in the slug and in the annular regimes are equated. This yields a relation for the transition superficial velocities. The evaluation of the annular flow void fraction requires the calculation of the interfacial shear at the liquid-gas interface of the annular flow. This is done using a Blasius type friction factor correlation. The Blasius correlation assumes no-slip of the relevant flow phase; whereas the gas does slip on the liquid. However, because typically $U_{GS} \gg U_{LS}$ in annular flow, the error from assuming that the gas does not slip may be small.

The arguments used to derive these boundaries hinge on a parameter C_o that appears in the drift-flow model. This parameter depends on whether the flow in the liquid is laminar or turbulent. The fact that the values of C_o chosen to adjust the data are not always consistent with the values prescribed based on the turbulence level of the liquid, weakens the power of this technique.

3.3.2 Weber number criterion

The Weber number criterion postulates that at the slug-to-annular transition inertial and surface tension forces should both be important. This criterion uses the gas superficial Weber number. It postulates that at transition $We_G = U_{GS}^2 \, \rho_G \, D/\sigma \approx 1$. Bousman has tested this criterion with three different fluid systems and two pipe diameters. The changes in fluid systems test the effects of viscosity and surface tension. Changes in pipe diameter test, obviously, the dependence on D. A change in viscosity does not change We_G. If there were a dependency of the transition threshold on μ, it should appear as a shift in We_G between the two systems with different viscosities. The data hint at some viscosity dependence of the transition We_G, although it is difficult to be definite when the scatter is as large as in these data and no error bars are quoted. When the viscosity is constant and D and σ change, the transition We_G seems to hold more or less constant. This supports the Weber-number transition criterion. Comparing the Weber number criterion to the Suratman number criterion of Jaywardena *et al.* [1], the latter has a much sharper demarcation of the flow domains.

3.4 Flow regime transition mechanisms

Mechanistic explanations for regime transitions have been attempted for many years. Here we summarize the more relevant ones.

3.4.1 Mechanisms for bubble-slug and slug-annular transition

Two interrelated mechanisms that have been proposed [5] are: (i) coalescence of individual bubbles leading to spherical cap and Taylor bubbles. It is believed that the frequency of bubble collisions, necessary for their eventual coalescence, increases rapidly when the void fraction is larger than 0.2. This led to the belief that bubble-slug transitions occur at void fractions around 0.25. (ii) Since bubble coalescence is a

slow process that must be preceded by drainage of the intervening liquid film, it is not very clear that coalescence is the only factor – the coalescing bubbles must be held in place for a sufficiently long time without relative motion. Therefore it has been suggested that the existence of "void waves" which creates regions of large bubble concentration where bubble separation is inhibited is an essential step. Colin *et al.* [28] suggest that coalescence happens more readily in reduced gravity because of lack of relative motion between the gas and the liquid. Thus coalescing bubbles could be held in place longer in reduced gravity.

Jayawardena *et al.* [1] do not discuss any mechanisms for the transition of bubbly to slug flow or from slug to annular flow. It is significant that the data is correlated by the Suratman number, $Su = \frac{\rho_L D\sigma}{\mu_L^2}$. Su only depends on the properties of the liquid and the pipe diameter, and does not depend on the flow rates of the liquid or gas. Briefly, Su is a modified Reynolds number where the characteristic velocity is the "capillary" velocity σ/μ. Thus, increasing surface tension should be thought of as increasing inertia of the capillary-driven flow. There is a likely analogy with breakup of a liquid filament, where the stability limit is controlled by Su. This should be so because it is commonly believed that bubbly-slug and slug-annular transitions are governed by merging and coalescence of bubbles, which are surely influenced by surface tension (and perhaps viscosity).

Another issue concerning transition boundaries is the question of reversibility. Is the transition boundary from regime 1 to regime 2 the same as from regime 2 to regime 1? The experiments we have found do not address this question. Rather, the gas and liquid flow rates are dialed and the ensuing flow regime is interrogated by the diagnostic method of choice. In real situations, flow rates might change more or less gradually, inducing changes in flow regime. It is therefore of interest to determine whether the regime boundaries are hysteretic or not.

A qualitative or semi-quantitative understanding of the reason why the flow regime map advocated by Jayawardena *et al.* [1] is so successful needs to be determined. One important reason is that, once the mechanism is understood, extensions for non-negligible values of the Froude number can be contemplated, which will be very useful for predicting flow regime maps in partial gravity.

The effect of gravity on axial development of bubbly flows for low liquid Reynolds numbers in small diameter pipes was studied by Takamasa et al. [9, 24] by monitoring key flow parameters such as void fraction, interfacial area concentration, bubble Sauter mean diameter and bubble number density. The flow measurements were performed in an air-water system using a non-intrusive image processing method with three digital cameras placed at 5, 20 and 40 diameters along the pipe section. The microgravity tests were performed in the underground drop shaft facility at the Japanese Microgravity Center (JAMIC) providing 10s of reduced gravity environment with nearly negligible residuals between 10^{-4} and 10^{-5} g. The main mechanisms for transition from bubbly to slug flow were studied by examining bubble coalescence and breakup. Since for the relatively low Reynolds numbers that prevailed in these

studies, bubble breakup was minimal, the main driving force for flow transition was due to bubble coalescence. Considerable bubble coalescence was observed in both the 1g and reduced gravity experiments. Visual records indicate that in 1g the main mechanism for bubble coalescence is wake entrainment. Wake entrainment refers to the entrainment of a trailing bubble by the motion of a leading bubble in the liquid – the motion of the leading bubble sets up a flow in the liquid that tends to entrain other bubbles. In microgravity, however, there is no mechanism for relative motion of the liquid and gas; thus wake entrainment is absent. At low liquid Reynolds numbers, where the flow is basically laminar and the velocity profile is parabolic, Takamasa et al. report that velocity profile entrainment is the main mechanism for bubble coalescence. In normal as well as microgravity, due to the relatively low Reynolds numbers encountered, coalescence due to random collisions is minimal. Curiously, it seems that the relative contributions of velocity profile entrainment, in microgravity, and wake entrainment, in 1g, to bubble coalescence is the same. This results in nearly similar flow structure developments for the two environments leading to a decrease in the interfacial area concentration and an increase in the Sauter mean diameter along the pipe.

3.4.2 Alternative mechanistic approaches for predicting regime transitions

Currently, in most of the analyses and codes used for predicting the behavior and performance of two-phase thermal-hydraulic systems, the effects of the different interfacial structures that evolve as the system transitions between the flow regimes are incorporated through certain transition criteria dictated by predetermined flow regime maps such as the one shown in Figs 2 and 3. Unfortunately, in this approach, no time or length scale is inherently incorporated into the transition criteria. As a result, such an approach is not well suited for simulation of developing flows. To solve this problem more mechanistic approaches have been proposed in recent years. One of the methods with great potential is based on a mechanistic prediction of the changes that take place in the two-phase flow structure based on the solution of a transport equation for the interfacial area concentration [9, 24, 40]. A successful formulation of this methodology is likely to make a drastic improvement in the development of future two-phase flow models for both 1g and reduced gravity predictions.

4 Flow Regimes in Partial Gravity

Hurlbert *et al.* 2004 [41] presented data on hydrodynamic measurements for two-phase flows in Mars and Moon gravity conditions, obtained aboard the KC-135 aircraft. The data was obtained using dichlorodifluoromethane (R-12) as the working fluid flowing in a tube with an inner diameter of 11.1 mm. The simulated gravitational acceleration for Mars was approximately 0.38-g, and that for Moon was approximately 0.17-g. We note that the residual gravity was perpendicular to the direction of flow in the tube. Also an attempt was made to scale the effects of gravity to predict the behavior of two-phase flow using Euler ($\equiv \Delta p/(\rho U^2)$) and Froude numbers.

John McQuillen, of NASA Glenn Research Center, obtained data in the KC-135 aircraft in a two-phase flow rig with Lunar gravity. He used air and a 50-50 water-glycerin solution (fig. 4), air-water (fig. 5), and air-water plus Zonyl 0.5% (fig. 6). The addition of Zonyl to water affected the surface tension without changing the density or viscosity. Also, we note that the residual gravity was perpendicular to the direction of flow in the tube.

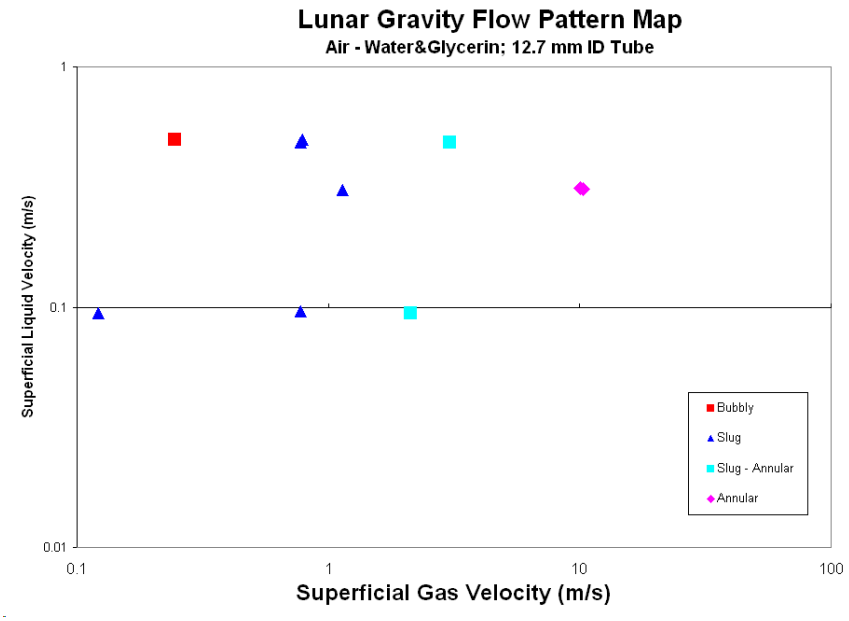

Figure 4: Flow map for Lunar gravity for Air and a 50-50 Water-Glycerin solution.

We describe next the current issues in the understanding of two-phase flow in normal gravity. Because gravity plays a very important role in two-phase flow, much of these issues are likely applicable in partial gravity conditions as well. Current state of knowledge on two-phase flow in normal gravity was discussed recently at a DOE workshop by members of the Study Group on Flow Regimes in the Workshop on Scientific Issues in Multiphase Flow Champaign-Urbana, IL [42],[43]. The findings at this workshop were published in four articles, and can be summarized as: (1) Phase Distribution in Gas-Liquid Flows where Theofanous *et al.* [44] identify pattern flow

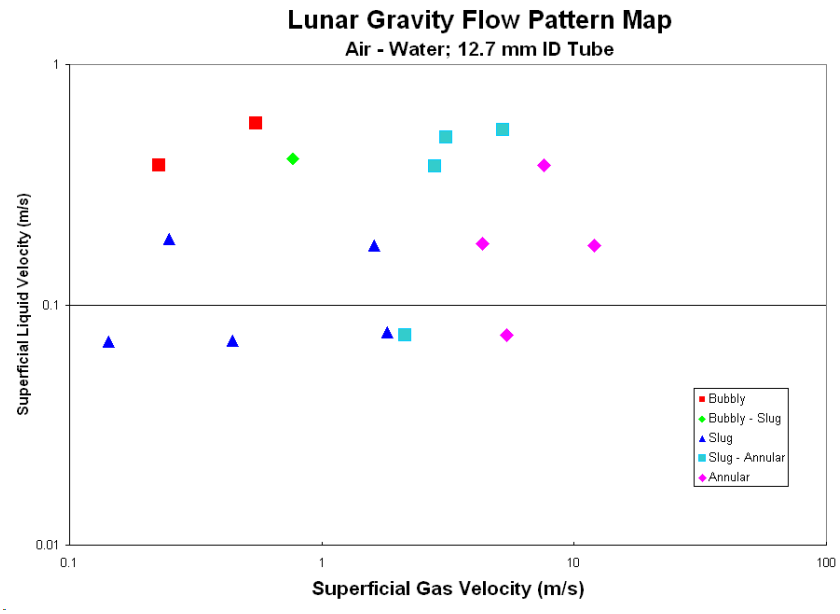

Figure 5: Flow map for Lunar gravity for Air-Water two-phase flow system.

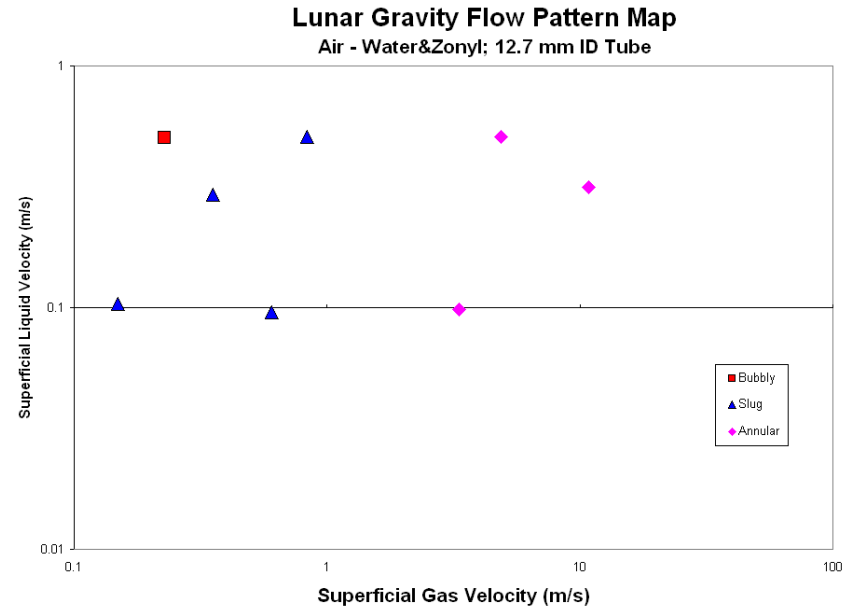

Figure 6: Flow map for Lunar gravity for Air-(Water-Zonyl mixture) two-phase flow system.

map as the principal scientific issue permeating essentially every aspect of multifluid flow. (2) For disperse flow, Sundaresan *et al.* [45] outlined a number of scientific challenges which represent building blocks for the comprehensive understanding of disperse flows encountered in a variety of technologies and in nature. We note that their report is heavily weighted toward solid-fluid interaction but the findings applied to fluid-gas interactions. (3) Prosperetti *et al.* [46] describe the advantages of Computational Physics besides its application to solving actual problems, as (a) a tool to develop and understand basic physics and as a guide toward asking more penetrating questions about two-phase flow (b) an aid in closing the averaged equations which are used to describe two-phase flow phenomena. Finally, (4) Delhaye *et al.* [47] summarize the role of microscopic phenomena in multiphase flow, specifically, the need to understand the coupling between molecular scale phenomena and macroscopic phenomena. These issues and those in Prosperetti *et al.* 2004 [48] are the current problems that need to be understood in 1-g.

In normal gravity two-phase flow, the inclination of the pipe, ϕ, becomes an important parameter. The flow regimes in vertical pipes are different from those in horizontal pipes. The flow regimes in horizontal pipes are (see fig. 7):

- Dispersed bubbly flow
- Plug flow
- Stratified flow
- Semi-slug flow
- Stratified wavy flow
- Slug flow
- Annular dispersed flow

The flow regimes in vertical pipes are (see fig. 8):

- Bubbly flow
- Slug or Plug flow
- Churn flow
- Annular flow
- Wispy annular flow

Thus gravity and its orientation are important parameters in two-phase flow. In the absence of gravity, principally only bubbly, slug and annular flow have been observed to occur. The flow regime map in microgravity is therefore relatively simplified.

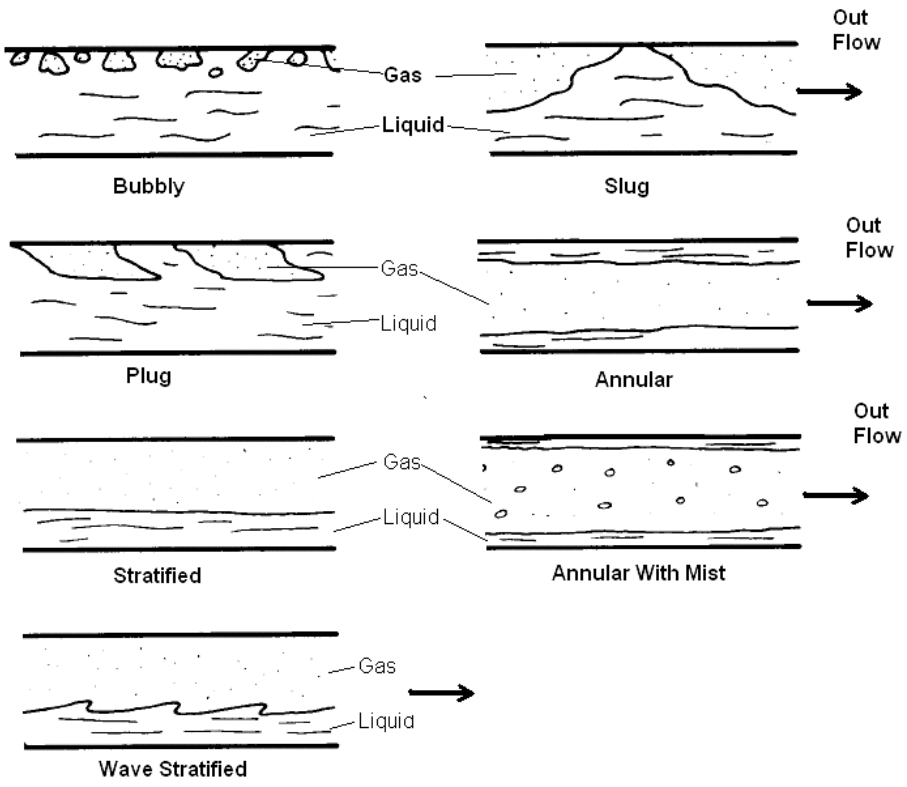

Figure 7: Flow patterns observed under normal gravity two-phase flows in a horizontal pipe.

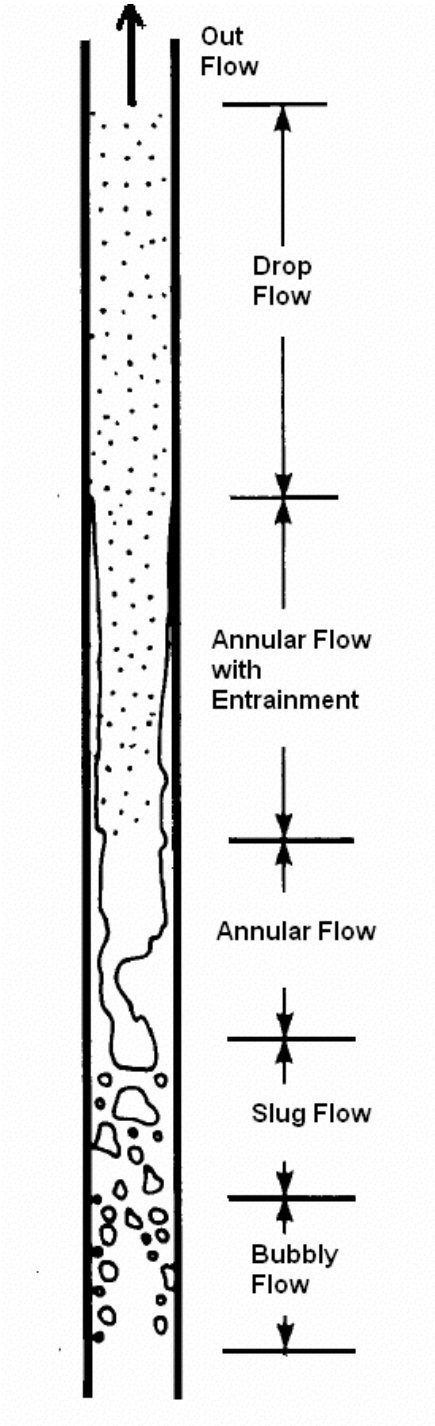

Figure 8: Flow patterns observed under normal gravity two-phase flows in a vertical pipe. Gravity direction is downwards.

5 Pressure Drop Predictions

The knowledge of pressure drop in a two-phase flow system is important for its design. It enables the designer to size the pump required for the operation of the flow system. We present below the most common approaches in prediction of the pressure drop in two-phase flows.

5.1 Homogeneous fluid model

The pressure gradient in a two-phase flow can be thought of as arising from three additive contributions: (i) frictional (ii) flow acceleration and (iii) hydrostatic head. Thus,

$$\frac{dp^*}{dz^*} = \left(\frac{dp^*}{dz^*}\right)_{fr} + \left(\frac{dp^*}{dz^*}\right)_{ac} + \left(\frac{dp^*}{dz^*}\right)_{gr} \tag{16}$$

In the homogeneous fluid model, the fluid is characterized by an effective fluid that has suitably averaged properties of the liquid and gas phases.

5.1.1 Pressure drop due to flow acceleration

The pressure gradient due to flow acceleration can be written as

$$\left(\frac{dp^*}{dz^*}\right)_{ac} = \frac{d}{dz^*}\left(\frac{1}{A}\int_A \rho u^2 dA\right) = \dot{m}^2 \frac{d}{dz^*}\left(\frac{1}{\rho_H}\right) \tag{17}$$

where $\dot{m}$ is the total rate of mass flow per unit area in the pipe, and the effective density ρ_H is defined by:

$$\rho_H = \epsilon_{GA}\rho_G + (1-\epsilon_{GA})\rho_L \tag{18}$$

where ϵ_{GA} is the area averaged local void fraction of the gas, ρ_G and ρ_L are the densities of the gas and the liquid.

5.1.2 Pressure drop due to gravity

The pressure gradient due to gravity may be written as

$$\left(\frac{dp^*}{dz^*}\right)_{gr} = g_z\rho_H = g_z[\epsilon_{GA}\rho_G + (1-\epsilon_{GA})\rho_L] \tag{19}$$

where g_z is the component of gravity in the z-direction.

5.1.3 Pressure drop due to wall friction

The frictional pressure drop due to the shear stress exerted by the tube wall is considered the most problematic term in two-phase pressure drop. The frictional pressure drop may be related to the wall shear stress τ_W by a force balance:

$$\left(\frac{dp^*}{dz^*}\right)_{fr} = \frac{2\tau_W^*}{R} \tag{20}$$

We present various approaches used in the literature to determine the frictional pressure drop.

Friction factor

Analogous to single phase flow, the use of friction factors in determining the two-phase frictional pressure drop is common. A typical expression for the friction factor f is given below.

$$\left(\frac{dp^*}{dz^*}\right)_{fr} = \frac{f\dot{m}^2}{\rho_H R}$$

$$f = 0.079 Re^{-0.25} \tag{21}$$

where the Reynolds number is $Re = \frac{2\dot{m}R}{\mu_H}$ with the effective viscosity approximated as [49]:

$$\mu_H = \mu_L \quad \text{or} \quad \mu_H = x\mu_G + (1-x)\mu_L \quad \text{or} \tag{22}$$

$$\frac{1}{\mu_H} = \frac{x}{\mu_G} + \frac{(1-x)}{\mu_L} \quad \text{or} \tag{23}$$

$$\mu_H = \beta\mu_G + (1-\beta)\mu_L \quad \text{or} \tag{24}$$

$$\mu_H = \mu_L(1-\beta)(1+2.5\beta) + \mu_G\beta \quad \text{or} \tag{25}$$

$$\mu_H = \frac{\mu_L\mu_G}{\mu_G + x^{1.4}(\mu_L - \mu_G)} \tag{26}$$

where x is the quality (the gas mass flow fraction).

Two-phase friction factor multiplier

Here the frictional pressure gradient for two-phase flow is determined by multiplying the frictional pressure gradient for flow of the liquid alone by a two-phase multiplication factor. The mass flow rate of the single phase liquid flow is the same as that of the liquid in the two-phase flow.

$$\left(\frac{dp^*}{dz^*}\right)_{fr,TP} = \phi_{LO}^2 \left(\frac{dp^*}{dz^*}\right)_{fr,LO} \tag{27}$$

where subscript TP denotes two-phase and LO liquid only. A typical correlation for the two-phase multiplier is

$$\phi_{LO}^2 = \frac{\rho_L}{\rho_H}\left[1 + x\frac{(\rho_L - \rho_G)}{\rho_G}\right]\left[1 + x\frac{(\mu_L - \mu_G)}{\mu_G}\right]^{-1/4} \tag{28}$$

5.2 Separated flow model

In this model the flow of the gas and vapor are analyzed as though the gas and liquid streams flow through separate tubes, with cross-section area proportional to the void fraction. To account for the interaction of the gas and the liquid, appropriate rates of transfer (*e.g.* mass, momentum or energy) are considered in the balance equations in a control volume formulation.

5.2.1 Pressure drop due to flow acceleration

The pressure gradient due to flow acceleration may be written as follows.

$$\left(\frac{dp^*}{dz^*}\right)_{ac} = \frac{d}{dz^*}\left(\frac{1}{A}\int_A \rho u^2 dA\right) = \dot{m}^2 \frac{d}{dz^*}\left(\frac{x^2}{\rho_G \epsilon_{GA}^2} + \frac{(1-x)^2}{\rho_L (1-\epsilon_{GA})^2}\right) \tag{29}$$

5.2.2 Pressure drop due to gravity

The expression for the pressure drop due to gravity is the same as that give for the homogeneous flow model.

5.2.3 Pressure drop due to wall friction

Lockhart-Martinelli correlation

The Lockhart-Martinelli correlation for the two-phase pressure gradient is similar in idea to the two-phase multiplier. A parameter X is defined as

$$X^2 = \frac{(dp^*/dz^*)_{LS}}{(dp^*/dz^*)_{GS}} \tag{30}$$

which is the ratio of the frictional pressure gradients for the liquid and gas alone, flowing at their respective superficial velocities. The single phase pressure drops are obtained using the Fanning equation that uses a friction factor:

$$\frac{dp^*}{dz^*} = \frac{f \rho U^2}{R}, \tag{31}$$

where:

$$f = \frac{16}{Re} \quad \text{for laminar flow,} \tag{32}$$

and for turbulent flow, two correlations are used:

$$f = \frac{0.079}{Re^{0.25}} \qquad Re \leq 2 \times 10^4, \quad \text{or} \tag{33}$$

$$f = \frac{0.046}{Re^{0.2}} \qquad Re \geq 2 \times 10^4 \tag{34}$$

where Re is based on pipe diameter i.e. $Re = \frac{\rho U D}{\mu}$ [50].

The two-phase frictional pressure gradient is then obtained by a multiplier defined as

$$\left(\frac{dp^*}{dz^*}\right)_{fr} = \phi_G^2 \left(\frac{dp^*}{dz^*}\right)_{GS} = \phi_L^2 \left(\frac{dp^*}{dz^*}\right)_{LS} \tag{35}$$

$$\phi_G^2 = 1 + CX + X^2 \quad \phi_L^2 = 1 + CX^{-1} + X^{-2} \tag{36}$$

where C is empirically determined and is in the range $5 < C < 20$. The value of C is 5 when the flow of liquid and gas is laminar and 20 when both flows are turbulent.

Friedel correlation

In the Friedel correlation, the two-phase multiplier ϕ_{LO} is calculated differently and the expression for it is given below.

$$\phi_{LO}^2 = E + \frac{3.24FH}{Fr^{0.045}We^{0.035}} \tag{37}$$

where

$$E = (1-x)^2 + x^2\left(\frac{\rho_L f_{GO}}{\rho_G f_{LO}}\right)$$

$$F = x^{0.78}(1-x)^{0.24}$$

$$H = \left(\frac{\rho_L}{\rho_G}\right)^{0.91}\left(\frac{\mu_G}{\mu_L}\right)^{0.19}\left(1-\frac{\mu_G}{\mu_L}\right)^{0.7}$$

$$Fr = \frac{\dot{m}^2}{2gR\rho_H^2}$$

$$We = \frac{2R\dot{m}^2}{\sigma\rho_H}$$

$$\rho_H \equiv \left(\frac{x}{\rho_G} + \frac{1-x}{\rho_L}\right)^{-1},$$

and f_{LO}, f_{GO} are the friction factors calculated as if the liquid and the gas respectively were flowing alone in the pipe (see M. M. Awad and Y. S. Muzychka, [51] where these parameters are defined).

5.3 Pressure drop in bubbly flow

The homogeneous and separated flow models do not consider the regime of the flow in order to predict the pressure drop. One would expect the pressure drop correlations to be tailored to the relevant flow regimes, but such correlations are not generally available.

In the case of bubbly flow in reduced gravity, Colin, Fabre and McQuillen (1996) [19] have determined that a friction factor approach correlates the experimentally

determined pressure drop quite well. Basically they find that a single-phase Blasius relationship for the friction factor works well when the liquid flow is turbulent.

$$\left(\frac{dp^*}{dz^*}\right)_{bub} = \frac{f_L \rho_L U_L^2}{R}, \quad f_L = 0.079 Re_L^{-0.25}, \quad U_L = \frac{U_{LS}}{1-\epsilon}, \quad Re_L = \frac{2\rho_L U_{LS} R}{\mu_L} \quad (38)$$

The predicted pressure drop is quite accurate for Re_L in the range 20,000 to 80,000. For Re_L less than 20,000 the experimentally obtained friction factor is larger than the above prediction. Further, in the case of single phase flow, a sharp increase in the friction factor is observed at a Reynolds number of around 8,000, where there is a transition from a laminar-like behavior to a turbulent-like behavior. Such a behavior is not observed for two phase flow.

An alternative approach that deserves consideration is to use a homogeneous fluid formulation with an effective viscosity μ_{eff} given by Einstein's viscosity for dispersions:

$$\mu_{\text{eff}} = \mu_L \left(1 + \phi \, \frac{\mu_L + \frac{5}{2}\mu_G}{\mu_L + \mu_G} + c_2 \, \phi^2\right),$$

where ϕ is the volume fraction of the gas bubbles and c_2 is a coefficient that must be determined experimentally [52]. We are not aware of the use of Einstein's viscosity for dispersions in the modeling of two-phase flows.

5.4 Pressure drop in slug flow

Colin, Fabre and McQuillen (1996) [19] comment that for slug flow, the above prediction for bubbly flow shows similar trends when compared to experimental results for slug flow. The data, however display much more scatter. There does not appear to be any other reliable prediction for the pressure drop in slug flow.

Sang Young Son and Jeff Allen [53] have studied pressure drop in two-phase flow through a square microchannel of 330μm side. The pressure drop found for slug flow increases as the gas flow rate increases and the flow transitions to "slug-annular". However, a further increase in gas flow rate causes a drastic decrease in pressure drop as the flow transitions to all-annular. This indicates that the extra pressure drop caused in slug flows by the presence of contact lines and/or thin lubricating films around gas bubbles is significant. Alternatively, one could think of this as the effective viscosity of the all-slug flow being higher than that of the all-annular flow for similar flow rates. This is analogous to the well-known fact that the effective viscosity of a foam (i.e., a collection of bubbles separated by very thin liquid layers) is much larger than the viscosity of either of its gas or liquid constituents. In circular channels, there are two types of slug flow: one type has continuous liquid phase through the presence of a lubricating liquid layer around each gas bubble (type 1); the other type has completely separate gas-liquid sections down the tube (type 2). The pressure drop in type 1 is less than in type 2, for the same flow rates and pipe size. In square channels, type 2 slug flow cannot exist because there is always liquid in the corners that connects the liquid all along the pipe. In this case, we can have

either type 1 when the liquid wholly surrounds each gas bubble, or a hybrid of types 1 and 2 when liquid exists around the bubble only in the corners while the rest of the bubble contacts dry channel wall.

Other works in pressure drop for two-phase flow in microchannels include Kawahara *et al.* [49] and Triplett *et al.* [54]. Microchannel flow work is important because it may provide information relevant to microgravity. However, one should keep in mind that just scaling the size down does not make a system similar to microgravity. Case in point, bubbly flow is widely documented in microgravity, but it is very difficult to observe bubbly flow (in the sense of having many bubbles across the tube cross section) in microchannels [54].

5.5 Pressure drop for fully developed, laminar, annular flow

For two-phase flow applications involved in advanced life support, the flow rates are expected to be somewhat low. Therefore, predictions of pressure drop etc., in laminar flow may be an appropriate baseline for such applications. Our analysis of fully developed annular flow when the flow is laminar is presented in Appendix A. The analysis reported there also includes the effect of gravity when $\mathbf{g}$ is parallel or antiparallel to the flow.

In fully developed annular flow there are two issues that need to be discussed concerning the structure and stability of the flow. First, there is the issue of which fluid flows next to the wall and which one flows in the center core. In all reduced gravity air-water flows that we are familiar with, water has been reported to be the fluid that is adjacent to the tube wall, and the gas is in the core. It has been suggested that in some two-phase flows a minimum dissipation principle is obeyed, which states that the less viscous fluid occupies the region where the shear stresses are the greatest [55]. In air-water flows, this principle would imply that air is in contact with the tube wall, which appears contrary to experimental observations. In Appendix B, we have proposed an argument based on the interfacial energy to develop criteria to determine which phase is in contact with the wall. For most gas-liquid annular flows, we find that the gas is indeed predicted to occupy the core and the liquid is in contact with the wall.

The second question is the position of the core center relative to the pipe center. We have pointed out in Appendix A that when the gas core is concentric with the axis of the tube, the total flow rate in the tube is a maximum for a fixed value of the pressure gradient.

5.5.1 Pressure drop due to flow acceleration

Flow acceleration occurs when the flow is developing, such as in entrance flows, or if there is a change in the flow geometry, such as when the flow encounters an expansion, contraction, or a bend. Flow acceleration can also be caused by phase change. In the case of fully developed flow, there is no flow acceleration. Therefore, strictly speaking, the pressure drop due to flow acceleration is zero. One might, however, approximate

the flow to be locally fully developed, with variations in z occurring over a much longer length scale than the length of pipe required to achieve fully developed flow. Using such an assumption, the pressure drop due to flow acceleration may be written as follows.

$$\left(\frac{dp^*}{dz^*}\right)_{ac} = \frac{d}{dz^*}\left(\frac{1}{A}\int_A \rho u^2 dA\right) \tag{39}$$

In eq. 39 all variables are dimensional. Using the pseudo velocity scale $w_{ps} = Q/\pi R^2$, and the pseudo length scale R,[3] we find

$$\left(\frac{dp^*}{dz^*}\right)_{ac} = \frac{-8Q^2}{\pi^2 \mu_L R^5}\frac{dR}{dz^*}\left[\rho_L \int_h^1 w_L^2 r dr + \rho_G \int_0^h w_G^2 r dr\right]. \tag{40}$$

All quantities in eq. 40 are dimensional except those in the integrals, where $w_L(r)$, $w_G(r)$ and h are the dimensionless quantities found in Appendix A. The integrals are independent of z under the assumption of locally fully developed flow (i.e., the wavelength of variations in z is $\gg R$). In figs. 9 and 10 we show the two integrals in eq. 40 for $M = 0.02$ (the viscosity ratio of air to water) as a function of h for various positive and negative values of F. The line $F = 0$ corresponds to zero-gravity. In fig. 11 we take advantage that, for large F, both Int_{Liq} and Int_{Gas} are $\sim F^2$. Thus, a single line independent of F represents accurately $Int_{Liq}F^{-2}$ and $Int_{Gas}F^{-2}$ uniformly in $0 < h < 1$.

Figures 9 to 11 show the integrals that appear in eq. 40 for virtually any F. From these graphs one can estimate pressure gradients due to acceleration in microgravity and in partial gravity. A negative F indicates that the direction of the vector $\mathbf{g}$ is opposite the axial coordinate direction in the pipe. For reference, in normal gravity, and assuming a 1 cm diameter pipe with characteristic liquid velocity of 1 cm/s, $F \sim 10^5$. Thus, Martian gravity corresponds to $F \sim 3 \times 10^4$ and Lunar gravity to $F \sim 1.5 \times 10^4$. These three cases are therefore covered by the large-F asymptotic behavior displayed in fig. 11. The microgravity case ($|F| \sim 0.1$) is covered in figs. 9 and 10.

5.5.2 Pressure drop due to wall friction in zero gravity

The results from Appendix A are specialized below when the effect of gravity is negligible by setting $F = 0$. The dimensional pressure gradient is

$$\left(\frac{dp^*}{dz^*}\right)_{fr} = \frac{8\mu_L U}{R^2}\frac{M}{h^4(M-1) - M} \tag{41}$$

where U is the total superficial velocity, $M = \frac{\mu_G}{\mu_L}$ is the viscosity ratio, and h (h must be less than 1) is obtained from

$$Q_{Gf} = \frac{h^4(2M-1) - 2Mh^2}{h^4(M-1) - M} \Rightarrow h = \left[\frac{[M(Q_{Gf}-1)\{M(Q_{Gf}-1) - Q_{Gf}\}]^{1/2} - M}{1 + M(Q_{Gf}-2) - Q_{Gf}}\right]^{1/2} \tag{42}$$

[3]We use the term "pseudo scale" to indicate that the scale is not a constant quantity but is a function of z through $R = \mathcal{R}(z)$.

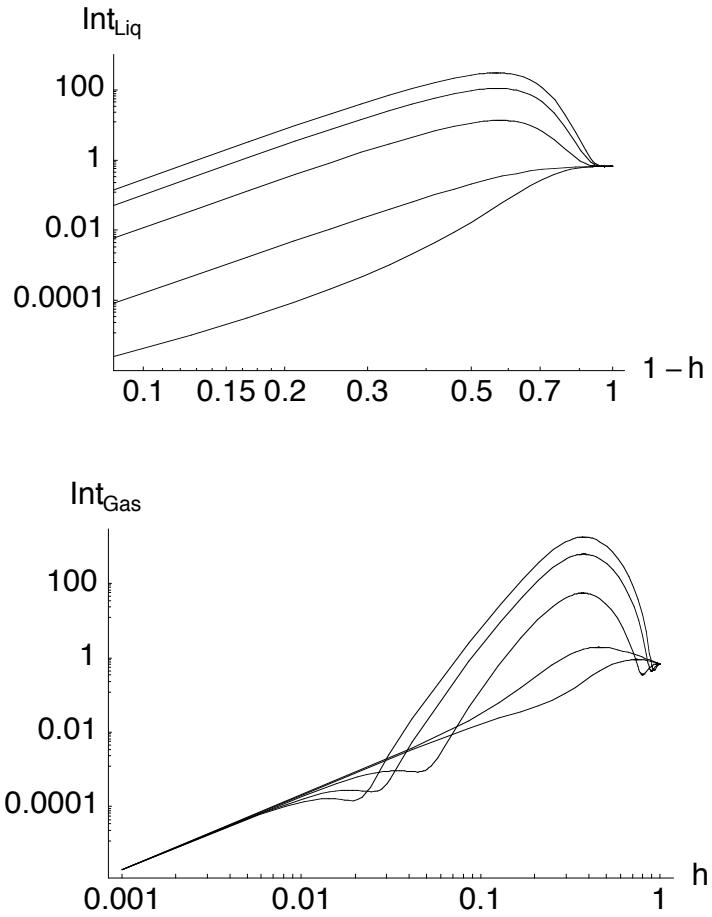

Figure 9: The integrals in eq. 40 as a function of h, for $M = 0.02$ and various values of $F = 0, 10, 100, 300, 500$. $F = 0$ corresponds to zero gravity. In Int_{Liq}, the lowest line is $F = 0$ and the highest is $F = 500$. In Int_{Gas}, the lines correspond to 10, 0, 100, 300, 500, in the order of increasing maxima. The asymptote of the gas integral is $Int_{Gas} \sim 2h^2$ for $h \ll 1$.

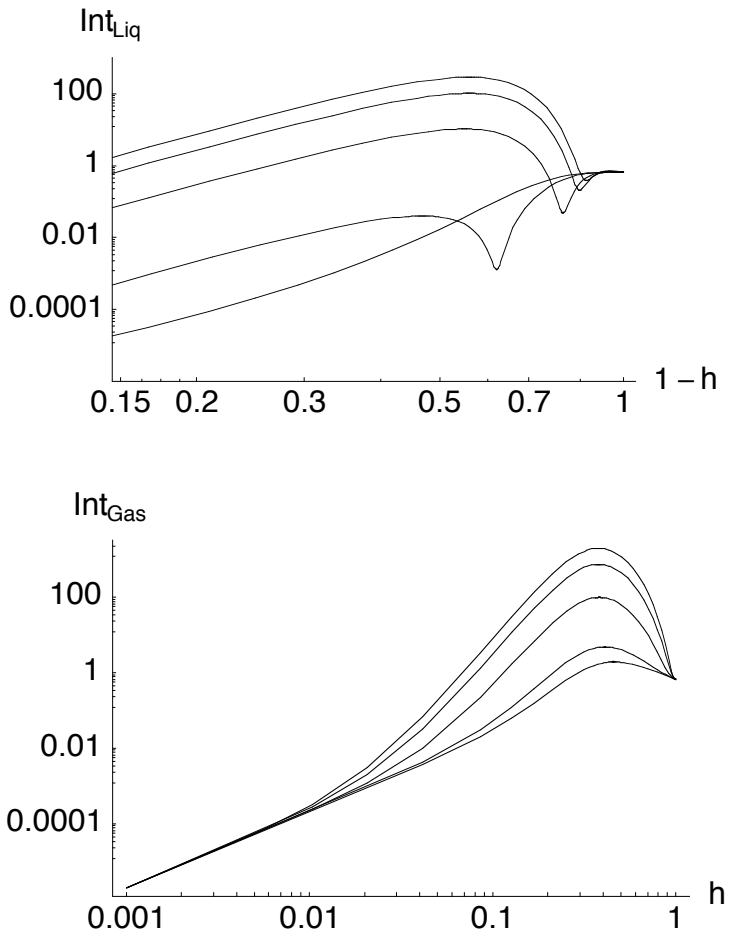

Figure 10: The integrals in eq. 40 as a function of h, for $M = 0.02$ and various values of $F = 0, -10, -100, -300, -500$. $F = 0$ corresponds to zero gravity. In Int_{Gas}, the lowest line is $F = 0$ and the highest is $F = -500$. In Int_{Liq}, the lines correspond to 0, -10, -100, 300, 500, from the lowest to the highest vertical axis intercepts. The asymptote of the gas integral $Int_{Gas} \sim 2h^2$ for $h \ll 1$.

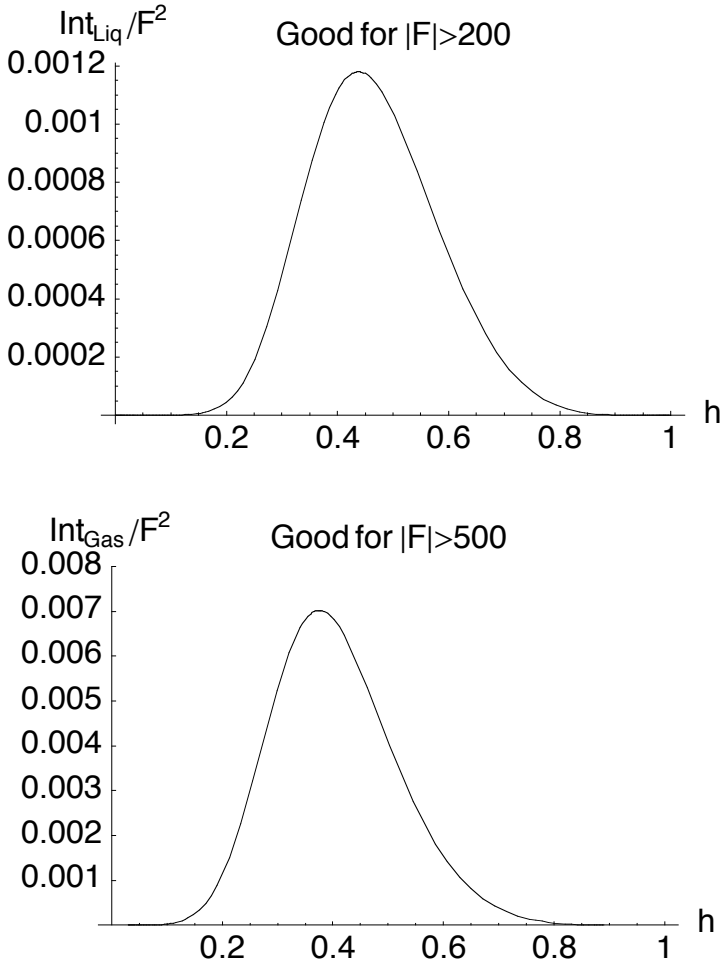

Figure 11: The integrals in eq. 40 as a function of h, for $M = 0.02$, valid for large $|F|$ as marked.

where Q_{Gf} is the gas volume flow fraction. The physical thickness of the liquid film adjacent to the tube wall is $R(1-h)$.

5.5.3 Pressure drop due to wall friction in partial gravity

In Appendix A we have plotted the pressure gradient in two plots (see figs. 16) according to the decomposition, obvious from eq. 58, $dp/dz = (dp/dz)_0 + F\,(dp/dz)_1$. From these graphs, the pressure gradient may be estimated for arbitrary values of the gravity parameter F.

5.5.4 Pressure drop in turbulent annular flow

The analysis we have performed in Appendix A can in principle be used for turbulent flow as well. Specifically, the relationship between the flow rate in the liquid film, the pressure gradient, and the liquid film thickness (often called the "triangular relationship", [56]) can be extended to the case of turbulent flow. Turbulent eddy-viscosity models are used for the transport of momentum in the thin liquid film. Numerical integration of the governing equations need to be performed to arrive at the triangular relationship. The reader is referred to literature by Hewitt, [56, 57] and [5] for further details.

5.6 Droplet entrainment in the air stream in annular flow

A key issue in annular flow is the entrainment of liquid droplets in the air stream. For the two-phase flow of air and water, annular flow naturally occurs when the air flow rate is large, with the velocity of the air in the core being considerably larger than the velocity of the liquid in the layer adjacent to the tube wall. When the relative phase velocity is large, interfacial waves with rather large amplitudes develop. As a consequence, especially when the air flow is turbulent, these waves break up portions of the interface into small droplets that are entrained and accelerated by the air stream. These droplets can also collide with the interface and be deposited back on the interface (see Hewitt and Govan, 1990, [58]). Because the air phase velocity is much larger than the liquid's, the total momentum when entrained liquid droplets flow in the air core is larger than otherwise. Therefore, the pressure drop with drop entrainment must be higher than the pressure drop without entrainment.

For flow under reduced gravity, Bousman *et al.* [23] suggest that droplet entrainment has an important and measurable role in the pressure drop. We have performed an integral momentum balance (reported in Appendix C) to obtain the effect of entrainment on the pressure drop. In this analysis, we have assumed that no droplets are present in the inlet gas stream, and that a fraction, f_{ent}, of the liquid film flow rate is entrained as droplets in the exiting gas flow. Hewitt and Govan (1990) [58] provide an empirical correlation for the entrainment fraction, but find considerable scatter when compared to experimental data. The pressure drop from Appendix C is provided below.

$$\Delta P = \frac{2\tau_W^* L}{R} + \rho_L U_{LS}^2 \left[f_{ent} \frac{U_{GS}}{U_{LS}} + (1 - f_{ent})^{3/2} \left(\frac{U_{GS}}{2U_{LS}} \right)^{1/2} \left(\frac{\mu_G}{\mu_L} \right)^{1/2} - 1 \right] \quad (43)$$

Using our notation, the correlation given by Hewitt and Govan, 1990, [58] for the entrainment rate is

$$f_{ent} = 5.75 \times 10^{-5} \, \frac{\rho_G U_{GS}}{\rho_L U_{LS}} \left[\frac{\rho_L^3 D}{\rho_G^2 \sigma} (U_{LS} - U_{LSF})^2 \right]^{0.316}$$

where

$$U_{LSF} = \frac{\mu_L}{\rho_L D} \, \exp\left(5.8504 + 0.4299 \, \frac{\mu_G}{\mu_L} \sqrt{\frac{\rho_L}{\rho_G}} \right)$$

5.7 Experimental measurements of pressure drop in annular flow

Bousman (1995) [3] performed experiments in reduced gravity aboard the NASA Learjet. Bousman used air-water, air-water/glycerin and air-water/zonyl as the fluid systems in the experiments. Water/glycerin mixture was used to study the effect of increase in viscosity and the surfactant zonyl was used to study the effect of reduction of surface tension.[4] The experiments were performed in a tube of internal diameter of 12.7 mm. Bousman compared the measured pressure drop in annular flow to predictions from the Lockhart-Martinelli correlation, and reports that this model is in agreement for all three fluids with an average error of $\pm$ 20% (see fig. 12). Bousman also recorded comparisons between the friction factor calculated from his measured pressure drops and the friction factor calculated using the standard relations 32-34, see figs. 13 and 14. He notes that, despite the "homogeneous" label of the model, he used μ_L to evaluate f (shown as f_{TP} in the figures' axes) because mostly liquid is in contact with the wall. Given the large scatter in the data it is hard to assess the goodness of the comparison besides the apparent observation that the calculated friction factor falls in the data cloud for slug flows but falls outside for bubbly and bubbly-slug flows. Bousman also indicates that separated flow models like the Lockhart-Martinelli predict poorly the pressure drops in bubbly and slug flows where the relative phase velocity is small. Earlier microgravity experiments by Miller *et al.* (1993) [59] found that in the case of freon R-12, the Lockhart-Martinelli model has an average error of 22% for flow in a tube of diameter 10.5 mm, but the error for a 4.6 mm tube is 56%.

[4] It is known that soluble surfactants –such as Zonyl– have dynamic effects besides lowering the surface tension. Dynamic effects arise from surfactant transport in the bulk and the free surface, and their coupling via adsorption kinetics. Dynamic effects will likely introduce deviations in interfacial deformation dynamics from the dynamics present if the surface tension were uniform.

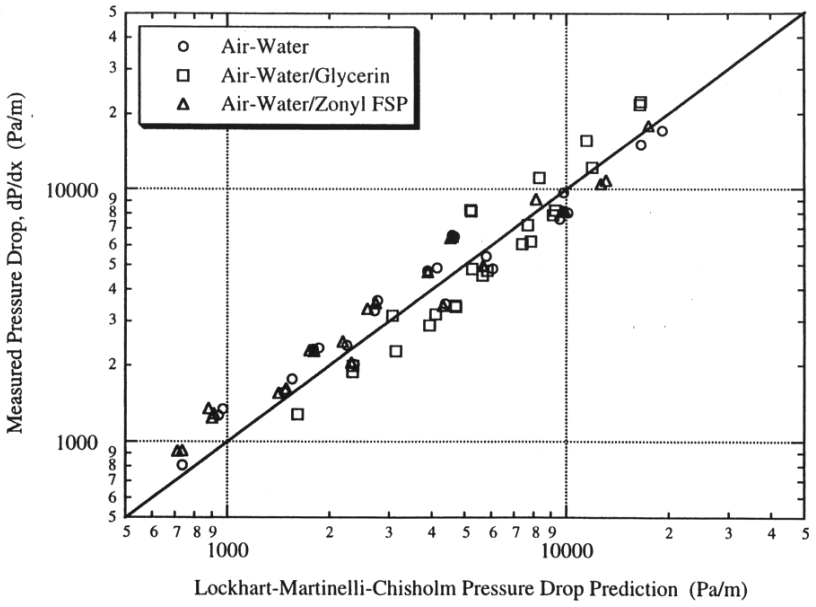

Figure 12: Bousman's [3] comparison between pressure drop in microgravity annular flow and the Lockhart-Martinelli prediction.

6 Heat Transfer in Fully Developed Annular Flow

In single fluid flow analyses, the relationship between wall heat transfer and wall friction has been exploited routinely to develop expressions for heat transfer coefficients from the friction factor data. For fully developed turbulent flow in a pipe with molecular and turbulent Prandtl numbers close to unity ($Pr = \frac{\nu}{\alpha}$, where $\nu = \mu/\rho$ is kinematic viscosity, and $\alpha = k/\rho\, c_p$ is thermal diffusivity), the assumption that heat and momentum are transported at the same rate produces the following relationship between the thermal and flow fields:

$$\frac{q^*}{c_p \tau^*} du = dT, \tag{44}$$

where q^* is heat flux normal to the wall and τ is shear stress. If, in addition, it is further assumed that the ratio of heat flux to shear stress is constant across the domain such that

$$\frac{q^*}{\tau^*} = \frac{q^*_W}{\tau^*_W},$$

where the subscript W denotes the quantity evaluated at the tube wall, eq. 44 can be integrated between the wall and mean bulk conditions to provide the following relationship between wall heat flux and shear stress:

$$\frac{q^*_W u_m}{\tau^*_W c_p} = T_W - T_b. \tag{45}$$

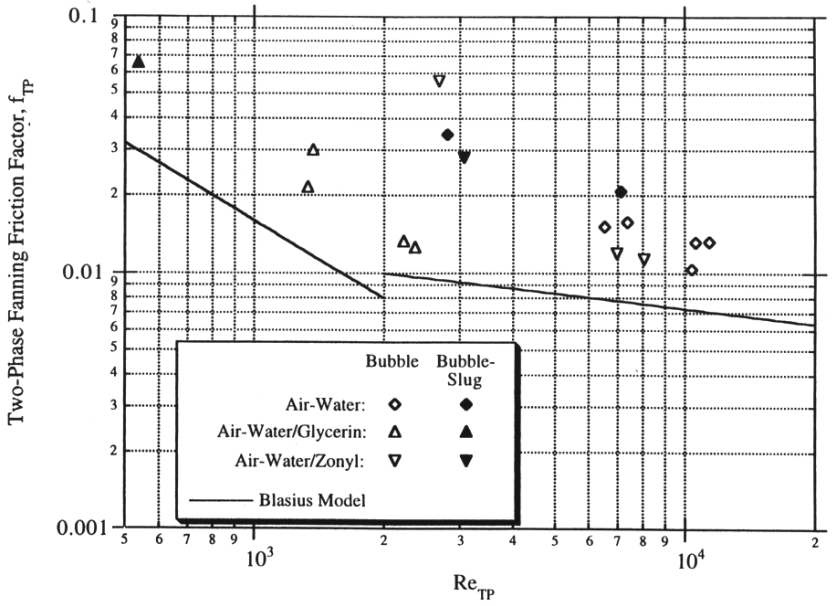

Figure 13: Bousman's [3] comparison between Fanning friction factor in microgravity bubbly and bubbly-slug flows and the homogeneous fluid prediction (eqs. 32-34 where the liquid viscosity μ_L is used.

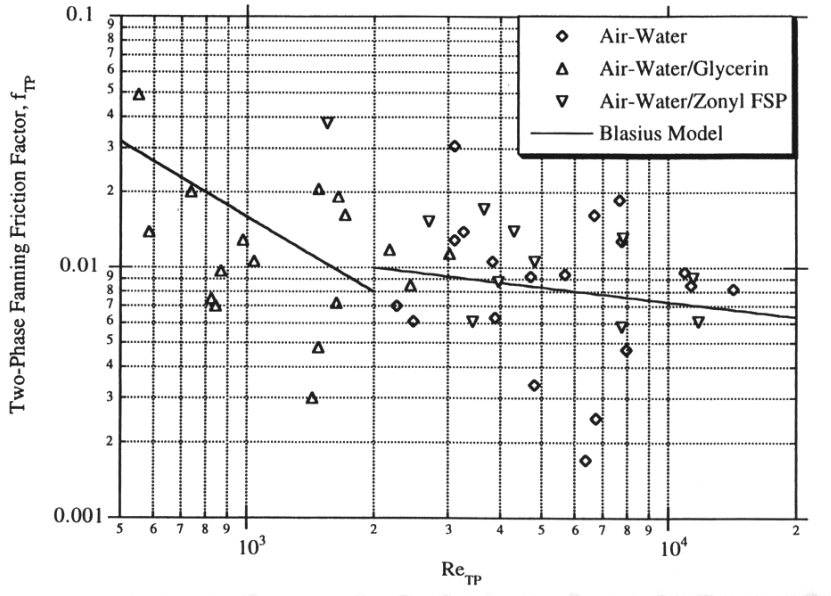

Figure 14: Bousman's [3] comparison between Fanning friction factor in microgravity slug flow and the homogeneous fluid prediction (eqs. 32-34 where the liquid viscosity μ_L is used.

Here u_m and T_b are the flow velocity and temperature outside the boundary layer respectively. When the definitions of heat transfer coefficient, $q^* = \tilde{h}(T_W - T_b)$, and Fanning friction factor, $\tau_W^* = \frac{f}{2}\rho u_m^2$ are substituted into eq. 45, a relationship between wall heat transfer and Fanning friction factor is derived:

$$St = \frac{f}{2}. \tag{46}$$

Here the Stanton number, St, represents the ratio of wall to convective heat transfer given by:

$$St \equiv \frac{\tilde{h}}{\rho c_p u_m}.$$

Equation 46 is called the Reynolds analogy for pipe flow and strictly speaking is only valid for fully developed turbulent pipe flows with molecular and turbulent Prandtl numbers equal to one [60]. A similar relationship between wall friction factor and heat transfer coefficient can be derived for turbulent and laminar boundary layer flows over a flat plate. This relationship is also known as the Colburn analogy [60]:

$$St\ Pr^{2/3} = \frac{f}{2}. \tag{47}$$

Colburn's analogy suggests that there is a Prandtl number dependence of $Pr^{2/3}$ for the flat plate problem. Curiously, it turns out this dependence also works well for turbulent pipe flows. Thus for turbulent pipe flows, a Reynolds analogy can be written that includes the Prandtl number dependence of the fluid in the form of eq. 47.

Even for single phase flows, one has to be cautioned that, while the friction-heat-transfer analogies can be applied to both laminar and turbulent flows over a flat plate and to turbulent pipe flows, they are not valid for laminar pipe flows and that, in general, more rigorous treatments of the governing equations and boundary conditions are needed when seeking new applications for these analogies. Specifically, Knudsen and Katz (1958) [61] have shown that for more generalized applications of the heat-transfer-fluid-friction analogies, the resulting expressions often do not take the simple forms represented by eq. 47.

Two-phase heat transfer in the fully developed laminar annular flow in pipes is amenable to analytical solution and an expression for the heat transfer coefficient can be derived as shown and described in Appendix B. Therefore, in two-phase flow, the heat-transfer fluid-friction analogy has been most widely applied to developed and developing turbulent annular flows. If the turbulent annular flow is fully developed and the thermal boundary layer is totally contained with in the liquid layer, then eq. 47 can be employed to estimate the heat transfer coefficient. For developing turbulent annular flows, application of Reynolds analogy becomes more involved. Chitti and Anand (1995) [62] have come up with an analytical procedure to derive the heat transfer coefficient through an iteration procedure for calculating film thickness. This procedure eliminates the need to calculate void fraction, pressure drop and

shear stress distribution. Instead, a distribution of heat flux in the radial direction is obtained by performing a steady state radial energy balance in the fluid and neglecting any axial contributions to heat transfer. The results indicate that the predicted values of the local heat transfer coefficient are within 25% of experimental data with a mean deviation of 15%.

The Reynolds analogy has been also been used rather loosely in some two-phase flow codes for piping systems. For example, the transient two-phase flow pipeline analysis code, TREMOLO, (Eliscon et al, 1999, [63]) uses Eq. 46 to calculate the heat transfer coefficient for annular flow, under any operating conditions. For plug flow, the model assumes that the phases contact the pipe wall in proportion to their volume fractions. The liquid phase heat transfer coefficient is then calculated according to eq. 46, while a constant condensation heat transfer coefficient is assumed for the vapor phase. The adequacy of such an approach to serve as a general procedure for calculating heat transfer coefficients for two-phase pipe flows is at best questionable.

Finally Ghajar (2004) [64] has pointed out the need for more systematic research in this area whereupon accurate isothermal pressure drop measurements are taken in the same regions where measured heat transfer data are available. The pressure drop data can then be used through a modified Reynolds analogy to back out heat transfer coefficients. By comparing the predicted heat transfer results against the experimentally measured heat transfer data, the correct form of the corresponding modified Reynolds analogy can be derived semi-empirically. In reality, this task needs to be undertaken for all the different two-phase flow regimes in 1g. Once the correct Reynolds analogy relationships are established for the two-phase pipe flows, they can then be conceivably used to obtain two-phase heat transfer data for regions and environments where, due to our experimental limitations, obtaining heat transfer data is not easily done.

7 Conclusions

In this report, we have presented a summary of flow regimes and pressure drop correlations that exist in the literature for two phase flow in a pipe, during operation in normal gravity, microgravity and partial gravity. While a lot of data exists for two phase flow in normal gravity, data for microgravity and especially partial gravity are scarce. Several applications of two phase flow in advanced life support systems for space applications suggest that the flow rates of gas and liquid are quite low compared to typical values in previous experiments. There is therefore a compelling need to revisit microgravity and partial gravity experiments and validate existing flow regime maps for the reduced flow rate conditions. In the case of laminar, fully-developed annular flow in a pipe, with the direction of flow and gravity being collinear, we find that the problem is amenable to rigorous mathematical treatment. Such a treatment has been extended to the heat transfer as well, when the wall heat flux is a constant. The effect of varying gravity level (Moon, Mars, microgravity) on the pressure drop and rate of heat transfer can be baselined from these analyses. There is a need to val-

idate these predictions, and the scalings (especially of the gravitational level) implied by these predictions, by appropriately designed experiments.

Appendix

A Fully developed, Laminar, Annular Flow

The goal is to predict the liquid film thickness, $R - h^*$, pressure gradient, $\frac{dp^*}{dz^*}$ and wall shear stress, τ_W, for given liquid and gas flow rates. Note that

- Liquid is adjacent to the wall, air is in the core of the flow, and g is oriented along the tube axis (z^* direction).
- The liquid and gas flow rates are specified to be Q_L and Q_G.
- Assume incompressible, laminar, axisymmetric, fully developed flow, and a constant liquid film thickness.

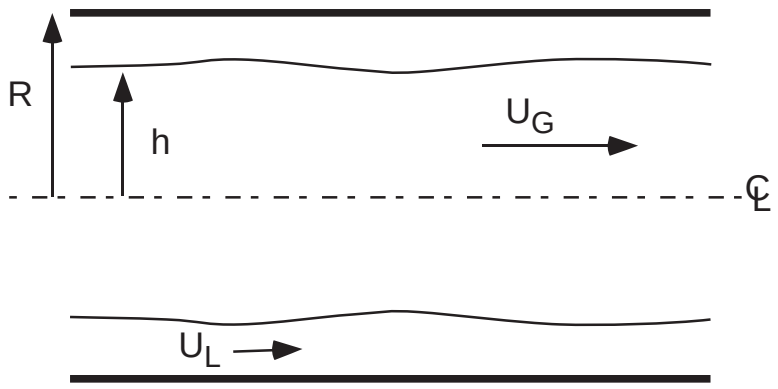

Figure 15: Schematic of fully developed annular flow with liquid annulus surrounding a gas core.

The governing equation for the flow in the liquid and gas is written below. A superscript * denotes a physical (dimensional) quantity.

$$0 = -\frac{dp^*}{dz^*} + \mu \frac{1}{r^*} \frac{d}{dr^*} \left(r^* \frac{dw^*}{dr^*} \right) + \rho \; g \tag{48}$$

The boundary conditions are

$$\frac{dw^*}{dr^*} = 0 \quad \text{at } r^* = 0 \tag{49}$$

$$w^* = 0 \quad \text{at } R^* = R \tag{50}$$

$$w^* \text{ and } \mu \frac{dw^*}{dr^*} \text{ are continuous at } r^* = h^* \tag{51}$$

Dimensionless variables are defined as follows.

$$w = \frac{w^*}{W_R}, \quad p = \frac{p^* - \rho_L g z^*}{P_R}, \quad r = \frac{r^*}{R}, \quad z = \frac{z^*}{R}, \quad h = \frac{h^*}{R}, \quad W_R = \frac{Q}{\pi R^2}$$

$$Q = Q_L + Q_G, \qquad P_R = \frac{\mu_L W_R}{R}, \qquad M = \frac{\mu_G}{\mu_L}, \qquad F = \frac{(\rho_L - \rho_G) g R^2}{\mu_L W_R} \tag{52}$$

For fully developed flow, the difference in pressure between the liquid and gas at any z location must be independent of z. Therefore, $\frac{dp_L}{dz} = \frac{dp_G}{dz}$ which will be denoted by $\frac{dp}{dz}$. The governing equation for the flow in the liquid and gas become

$$\frac{1}{r}\frac{d}{dr}\left(r\frac{dw_L}{dr}\right) = \frac{dp}{dz} \qquad h \le r \le 1 \tag{53}$$

$$\frac{1}{r}\frac{d}{dr}\left(r\frac{dw_G}{dr}\right) = \frac{1}{M}\frac{dp}{dz} + \frac{F}{M} \qquad 0 \le r \le h \tag{54}$$

The solution is

$$w_L = \frac{1}{4}\frac{dp}{dz}(r^2 - 1) + \frac{1}{2}F\ h^2 \ln r \tag{55}$$

$$w_G = \frac{1}{4}\frac{dp}{dz}\left[h^2\left(1 - \frac{1}{M}\right) - 1 + \frac{r^2}{M}\right] + \frac{F}{4\,M}[r^2 + h^2(2M \ln h - 1)] \tag{56}$$

The liquid film thickness and the pressure gradient are determined from the following equations:

$$\begin{aligned} Q_{Gf} = {} & \frac{h^4(2M-1) - 2Mh^2}{h^4(M-1) - M} + \\ & \frac{1}{2}Fh^4 \ln h - \frac{F}{8}\frac{h^4(h^2-1)[h^2(4M-3) - 4M + 1]}{h^4(M-1) - M} \end{aligned} \tag{57}$$

$$\frac{dp}{dz} = \frac{8M - h^2 F\,[h^2(2M-1) - 2M]}{h^4(M-1) - M} \tag{58}$$

where $Q_{Gf} = \frac{Q_G}{Q}$ and $Q_G = 2\pi \int_0^h w_G\, r\, dr$. The shear stress exerted by the wall onto the fluid, $\tau_W^* = \tau_{rz}^*$ is [5]

$$\tau_W^* = \mu_L \left(\frac{dw_L^*}{dr^*}\right)_W = \frac{\mu_L W_R}{R}\left(\frac{dw_L}{dr}\right)_{r=1} = \frac{1}{2}\frac{\mu_L W_R}{R}\left(\frac{dp}{dz} + Fh^2\right) \tag{59}$$

[5] In order to get the signs correct, $\frac{\Delta P}{L}$ should be interpreted as $\frac{dp}{dz}$ and τ_W is positive when it points along the negative z direction.

Note that the physical pressure gradient is

$$\frac{dp^*}{dz^*} = \rho_L g + \frac{P_R}{R}\frac{dp}{dz} \tag{60}$$

Using dp/dz given in eq. 59, and inserting the definition of $P_R \equiv \mu_L W_R/R$, we find

$$\begin{aligned}\frac{dp^*}{dz^*} &= \rho_L g + \frac{\mu_L W_R}{R^2}\left[\frac{2\tau_W^* R}{\mu_L W_R} - Fh^2\right] = \rho_L g + \frac{2\tau_W^*}{R} - \frac{\mu_L W_R}{R^2}Fh^2 = \\ &\rho_L g + \frac{2\tau_W^*}{R} - \Delta\rho g h^2 = g\left[\rho_L(1-h^2) + \rho_G h^2\right] + \frac{2\tau_W^*}{R}\end{aligned} \tag{61}$$

In other words, the physical pressure gradient is composed of the wall shear and a gravity component with an effective density

$$\rho_{eff} \equiv \rho_L(1-h^2) + \rho_G h^2 \tag{62}$$

The area fractions of gas and liquid are h^2 and $1-h^2$ respectively. Eq. 62 is an exact result for fully developed annular flow. It shows that the averaging that yields the effective density must be weighted with the phase area fractions given above. As expected, the result

$$\frac{dp^*}{dz^*} = g\left[\rho_L(1-h^2) + \rho_G h^2\right] + \frac{2\tau_W^*}{R} \tag{63}$$

agrees with the force balance around a control volume of the annular flow. The pressure gradient is balanced by the weight and the drag that the wall exerts on the liquid. The results for the gravitational and frictional pressure gradient given above are in accord with those given in Section 5.1.

In figs. 16 we plot the two components of the pressure gradient given in eq. 58. $(dp/dz)_0$ shows the purely viscous part, obtained for $F = 0$; whereas $(dp/dz)_1$ shows the gravitational part, given by the coefficient of F; refer to eq. 58. With these two figures we can calculate pressure gradients for arbitrary F. Similarly, in figs. 17 we show $Q_{gf_0} = Q_{gf}(F = 0)$ and the coefficient of F, Q_{gf_1}. For arbitrary F, $Q_{gf} = Q_{gf_0} + FQ_{gf_1}$.

For most parameter ranges, there is a unique h for each Q_{gf} and M. However, we note that, in certain ranges of F for given M, there exist more than one h for given Q_{gf}. This is illustrated in fig. 18, where we show Q_{gf} for $M = 0.02$ and $F = 18$. Depending on Q_{gf}, there may be one, two or three values of h that satisfy eq. 57. The implications of this multiplicity in film thickness for fixed gas flow fraction are not clear at this time and will be addressed later during the course of this project. Nevertheless, for $Q_{gf} \gtrsim 0.5$ for which annular flow can be expected to occur, the film thickness is uniquely determined.

A.1 Core phase center relative to pipe center

It may be shown that, for a given pressure gradient, dp/dz, the maximum total flow rate $Q_L + Q_G$ is obtained when the center fluid core is concentric with the pipe. Any eccentricity causes the total flow rate to fall below the concentric case maximum.

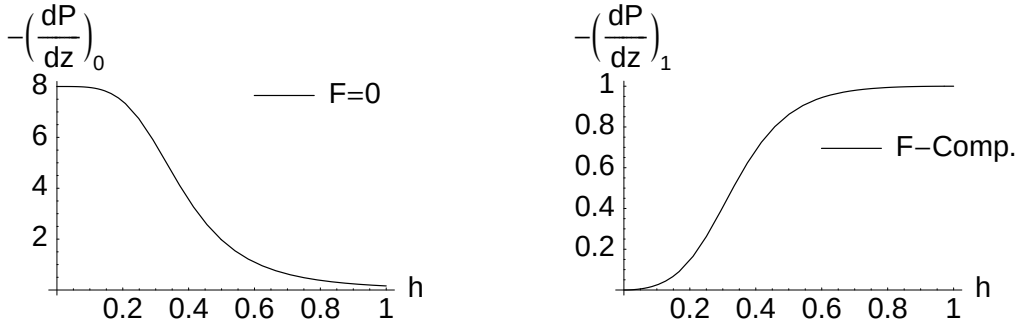

Figure 16: The purely viscous ($(dp/dz)_0 \equiv dp/dz$ for $F = 0$) and gravitational (the coefficient of F in eq. 58) components of the pressure gradient. $M = 0.02$. To get dp/dz for arbitrary F one should add $(dp/dz)_0 + F\,(dp/dz)_1$.

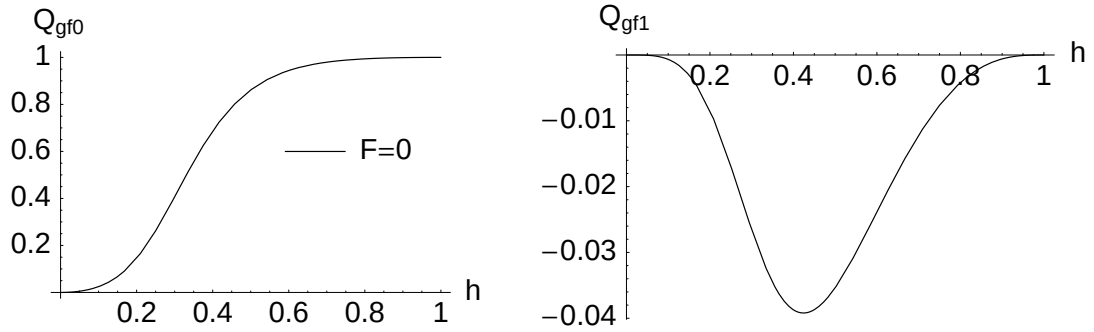

Figure 17: The purely viscous ($Q_{gf_0} \equiv Q_{gf}$ for $F = 0$) and gravitational (the coefficient of F in eq. 57) components of Q_{gf}. $M = 0.02$. To get Q_{gf} for arbitrary F one should add $Q_{gf_0} + F\,Q_{gf_1}$.

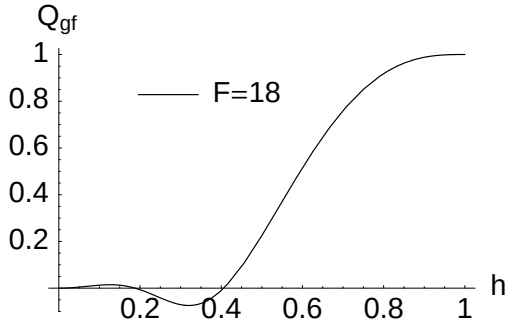

Figure 18: Q_{gf} for $M = 0.02$ and $F = 18$.

B Heat Transfer in Fully Developed Annular Flow

The results given in the Appendix A can be used to determine the heat transfer in fully developed annular flow. We assume that a constant heat flux per unit wall area, q^*, is imposed at the tube wall. The goal is to obtain the Nusselt number, defined as $Nu \equiv \tilde{h}R/k_L$, where $\tilde{h}$ is the heat transfer coefficient, R the pipe radius and k_L the liquid's thermal conductivity.
We begin by writing the steady state energy equation:

$$w^* \frac{\partial T^*}{\partial z^*} = \alpha \left[\frac{\partial^2 T^*}{\partial z^{*2}} + \frac{1}{r^*} \frac{\partial}{\partial r^*} \left(r^* \frac{\partial T^*}{\partial r^*} \right) \right] \tag{64}$$

where $\alpha \equiv k/\rho\, c_p$ denotes the thermal diffusivity, with c_p being the fluid's heat capacity. The axial velocity field w^* depends only on the radial coordinate, r^*, and is given in Appendix A.

Because the rate of heat input along the wall is constant with z^*, we anticipate that the temperature field $T^*(r^*, z^*)$ will be the sum of a function of r^* plus a linear function of z^*. We will show that a constant axial temperature gradient G is established by the imposed wall heat flux. G will be determined as a part of the solution. Based on these ideas, we seek a solution where the temperature field is written as follows:

$$T(r) \equiv \frac{T^*(r^*, z^*) - Gz^*}{GR} \tag{65}$$

where $T(r)$ is dimensionless. With this substitution, the energy equation in each phase becomes:

$$Pe_L \; w_L(r) = \frac{1}{r} \frac{d}{dr} \left(r \frac{dT_L}{dr} \right) \tag{66}$$

$$Pe_G \; w_G(r) = \frac{1}{r} \frac{d}{dr} \left(r \frac{dT_G}{dr} \right) \tag{67}$$

where $Pe_{(G,L)} = \frac{w_R R}{\alpha_{(G,L)}}$ is the Péclet number of the gas or the liquid. The boundary conditions are: a constant heat flux, $q \equiv q^*/k_L G$ is imposed at the tube wall, the temperature field is symmetric about the axis of the tube, and the temperature and heat flux are continuous across the liquid/gas interface.

$$\frac{dT}{dr} = q \quad \text{at } r = 1 \tag{68}$$

$$\frac{dT}{dr} = 0 \quad \text{at } r = 0 \tag{69}$$

$$T_L = T_G \text{ at } r = h \tag{70}$$

$$\beta \frac{dT_G}{dr} = \frac{dT_L}{dr} \text{ at } r = h \tag{71}$$

where $q \equiv \frac{q^*}{k_L G}$ and $\beta \equiv \frac{k_G}{k_L}$ is the thermal conductivity ratio. In this analysis the temperature field depends only on temperature differences and/or gradients. Thus, $T_{(G,L)}(r)$ can only be determined up to an additive constant. To choose one value for this constant, we set $T_L(1)$ to be zero. With these boundary conditions, the solution is

$$\begin{aligned} T_L &= \frac{Pe_L}{8}\left\{FMh^2\left[1-r^2+\ln r\left(r^2+h^2(1-2\ln h)\right)\right]+\right. \\ &\qquad \left.\frac{dp}{dz}\left[h^2\ln r(1-\frac{h^2}{2})+(r^2-1)(r^2-3)\right]\right\}+ \\ &\quad \frac{Pe_G\,\beta}{8}\left\{2Fh^4\ln r\left[M\ln h-\frac{1}{4}\right]+\frac{dp}{dz}h^2\ln r\left[h^2\left(1-\frac{1}{2M}\right)-1\right]\right\} \end{aligned} \tag{72}$$

$$\begin{aligned} T_G &= \frac{Pe_L}{8}\left\{FMh^2\left[1+h^2\left(-1+2\ln h(1-\ln h)\right)\right]+\right. \\ &\qquad \left.\frac{1}{2}\frac{dp}{dz}\left[\frac{3}{4}+h^2\left(\frac{h^4}{4}-1\right)+h^2\ln h(2-h^2)\right]\right\}+ \\ &\quad \frac{Pe_G}{8}\left\{F\left[h^2M\ln h(r^2-h^2+2\beta h^2\ln h)+\frac{1}{8}\left((h^2-r^2)(3h^2-r^2)-4\beta h^4\ln h\right)\right]+\right. \\ &\qquad \left.\frac{1}{2}\frac{dp}{dz}\left[(h^2-1)(r^2-h^2+2\beta h^2\ln h)+\frac{(h^2-r^2)(3h^3-r^2)-4\beta h^4\ln h}{4M}\right]\right\}, \end{aligned} \tag{73}$$

where $\frac{dp}{dz}$ is given by eq. 58. By applying the heat flux boundary condition, $-q = dT/dr$ at $r = 1$, we determine the unknown axial temperature gradient G from:

$$\frac{q^*}{k_L G} = q = \frac{1}{2}\left[Pe_L(1-Q_{GF})+\beta Pe_G Q_{GF}\right]. \tag{74}$$

Noting that $\beta Pe_G = Pe_L \frac{\rho_G\, c_{p_G}}{\rho_L\, c_{p_L}}$, we conclude that both T_G and T_L are proportional to Pe_L, and depend on the heat capacity ratio $\frac{\rho_G\, c_{p_G}}{\rho_L\, c_{p_L}}$ and β in a more complex manner. This is useful, because then Pe_L is the only parameter that contains flow rate in the expressions for temperature.

To compute the Nusselt number we start from the expression $\tilde{h}(T^*_W - T^*_{AV}) = -q^*$. The average temperature in the fluid is defined as

$$T^*_{AV} = \frac{\int_A \rho\, c_P w^* T^* dA}{\int_A \rho\, c_P w^* dA}.$$

The weighting by ρc_p defines an average temperature that closely reflects the actual average temperature in an instantaneous sample of a cross sectional slice of the flow. In other words, a representative average temperature cannot come from an arithmetic average over the cross sectional area. This is because the change in fluid temperature by the heat input q^* must depend on heat capacity: for example, if $\rho_G c_{p_G} = 0$, the

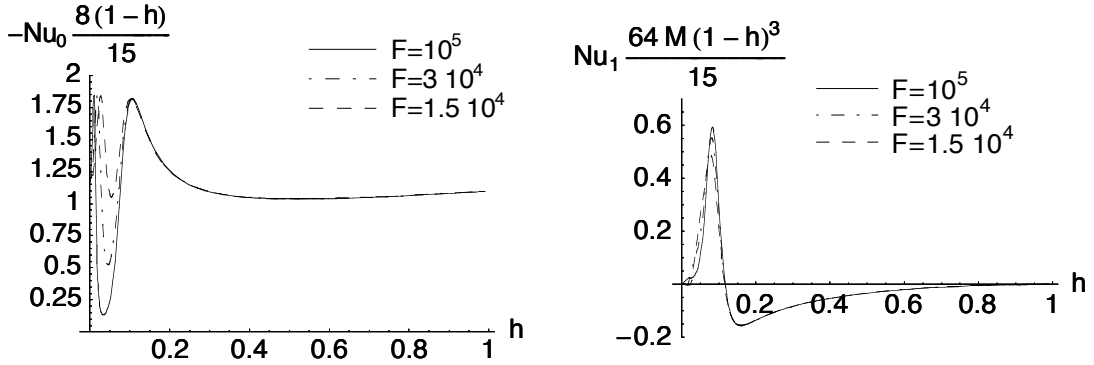

Figure 19: Coefficients Nu_0 and Nu_1 as defined in eq. 76, for F values as marked, and $M = 0.02$. The horizontal axis, h, is the radius of the gas core. The values of F represent, in decreasing order, Earth's, Mars' and Moon's gravity levels.

gas cannot accept heat and therefore T_G does not change in the streamwise direction; however, the liquid temperature increases more rapidly than if $\rho_G c_{p_G} \neq 0$ because then all the heat input q^* goes to the liquid.

Making the preceding expression dimensionless, and evaluating $q^* = -k(\partial T/\partial r)|_W$,

$$Nu\ (T_W - T_{AV}) = \left.\frac{\partial T}{\partial r}\right|_W \tag{75}$$

Thus, the Nusselt number can be calculated after solving for $T(r)$. In general, $Nu = f(h, F, M, \beta, \frac{\rho_G\, c_{p_G}}{\rho_L\, c_{p_L}})$. The expression was worked out in Mathematica and it's too complicated to be written here. However, we have analyzed one relevant limiting case, $\frac{\rho_G\, c_{p_G}}{\rho_L\, c_{p_L}} \to 0$ up to order $\mathrm{O}\left(\frac{\rho_G\, c_{p_G}}{\rho_L\, c_{p_L}}\right)$. We assume the following Taylor series:

$$Nu(h, F, M, \beta, \frac{\rho_G\, c_{p_G}}{\rho_L\, c_{p_L}}) = Nu_0(h, F, M) + \frac{\rho_G\, c_{p_G}}{\rho_L\, c_{p_L}} Nu_1(h, F, M) + ... \tag{76}$$

Interestingly, up to this order of approximation, the dependence on β disappears exactly.

For illustration purposes, we show in figs. 19 through 22 the two coefficients of eq. 76 for $M = 0.02$ (the viscosity ratio of air to water), for various F positive and negative, and $0 \leq h \leq 1$. Since $Nu_0 \sim (1-h)^{-1}$ and $Nu_1 \sim (1-h)^{-3}$ as $h \to 1$, we plot each term multiplied by its divergent behavior to suppress the singularity and thus make the plot bounded. Note that the coefficients are quite insensitive to the gravitational parameter F in a broad range of $F \gg 1$:

B.1 Criterion for phase in contact with wall

Assume that liquid and gas flow rates Q_L, Q_G are injected into a pipe of radius R. Assume, further, that these parameters together with the fluid properties are such

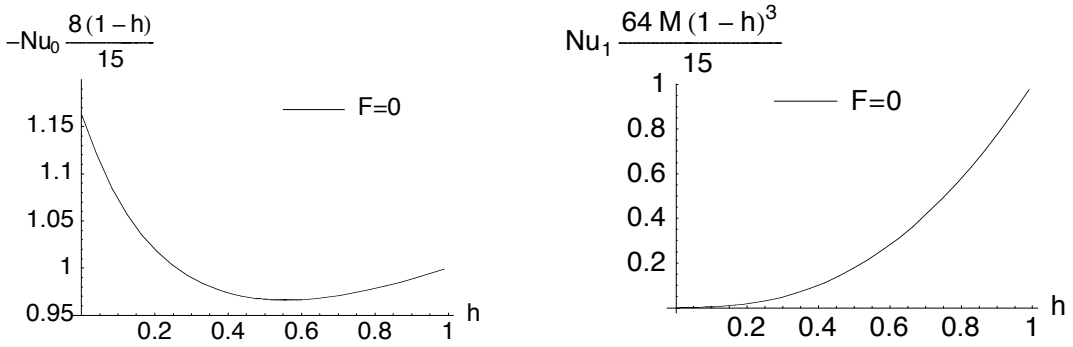

Figure 20: Coefficients Nu_0 and Nu_1 as defined in eq. 76, for $F = 0$ (zero gravity).

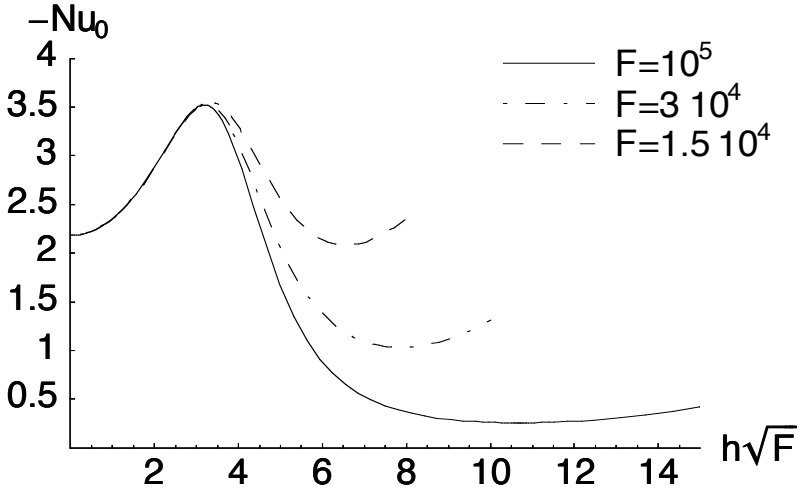

Figure 21: Coefficient Nu_0 near $h = 0$ for F values as in fig. 19.

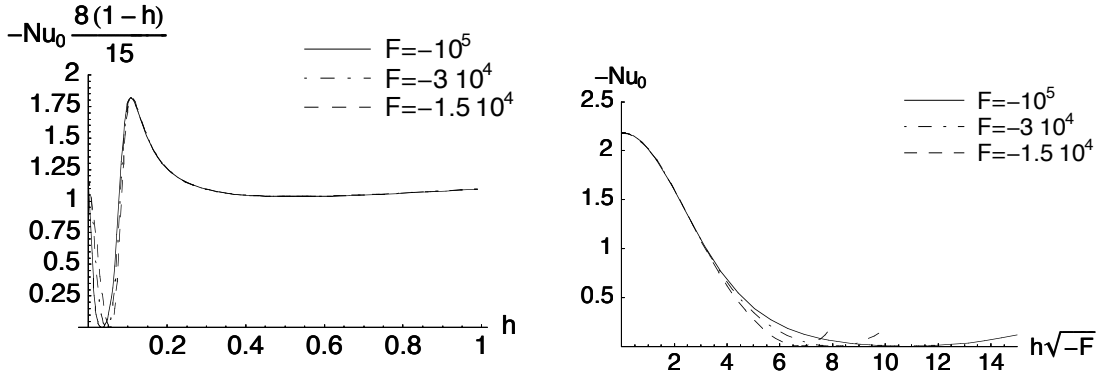

Figure 22: Coefficient $Nu_0$for negative F values as in fig. 19. The plot on the right shows a detail near $h = 0$; note the scaled h variable.

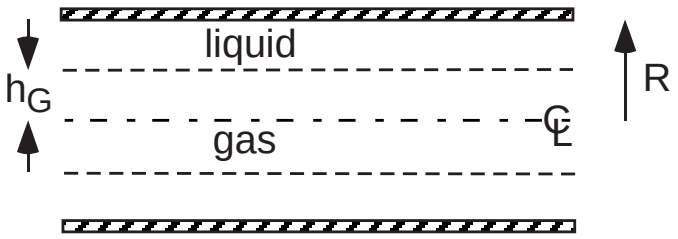

Figure 23: Schematic of a fully developed annular flow with gas center core of radius h_G. If liquid flows in the center, then its core radius would be h_L.

that conditions for annular flow are met. Even in this case, the operator has no control over the phase distribution within the pipe. Which fluid flows next to the wall –and which one in the core– is selected by the system without the operator's intervention. Here we propose an argument based on the interfacial energy of the system that begins to address this question.

Refer to fig. 23. h_L and h_G refer respectively to the core radii of the liquid or the gas, depending on whether liquid or gas flows in the core. We evaluate the interfacial energies of the two possible configurations. The quantities, E_{GC} and E_{LC} refer to the interfacial energies per unit pipe length of the system with gas core and liquid core, respectively:

1) Gas core: $E_{GC} = 2\pi\,(R\;\sigma_{SL} + h_G\;\sigma)$.

2) Liquid core: $E_{LC} = 2\pi\,(R\;\sigma_{SG} + h_L\;\sigma)$.

Subtracting the two expressions, $E_{GC} - E_{LC} = 2\pi\,[R\,(\sigma_{SL} - \sigma_{SG}) + (h_G - h_L)\sigma]$.

Here, σ_{SL} and σ_{SG} are the interfacial energies per unit area of the solid-liquid and the solid-gas interfaces, respectively; and σ is the liquid-gas interfacial tension. Young's equation relates these three quantities to the contact angle, θ: $\sigma\cos\theta = \sigma_{SG} - \sigma_{SL}$. Inserting this into the previous expression we obtain:

$$E_{GC} - E_{LC} = 2\pi\sigma\,[-R\cos\theta + (h_G - h_L)] \tag{77}$$

The energy principle states that the lowest energy state is most favorable. This implies that gas core should be expected when $E_{GC} - E_{LC} < 0$, and liquid core when $E_{GC} - E_{LC} > 0$. In terms of the contact angle,

$$\text{Gas Core}: \qquad \cos\theta > \frac{h_G - h_L}{R}. \tag{78}$$

$$\text{Liquid Core}: \quad \cos\theta < \frac{h_G - h_L}{R}. \tag{79}$$

In fig. 24, we can see that, for air-water ($M = \frac{\mu_G}{\mu_L} = 0.02$), the gas core is thicker

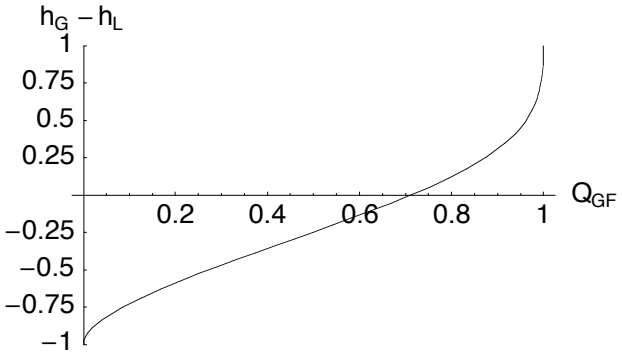

Figure 24: Difference if gas and liquid core radii normalized by pipe radius R, as a function of gas flow rate fraction, Q_{GF} for $M = \mu_G/\mu_L = 0.02$. h_G is calculated with eq. 42; h_L is obtained from the same equation, by replacing M by M^{-1} and Q_{GF} by $1 - Q_{GF}$.

than the liquid core (i.e., $h_G > h_L$) if $Q_{GF} \gtrsim 0.71$. Then the right-hand side of eq. 78 is positive. This condition is met in most gas-liquid annular flows.

From these expressions we conclude that, for example, in order to have liquid next to the wall (i.e., gas core) with $Q_{GF} \gtrsim 0.71$, having a wetting liquid (i.e., $\cos\theta > 0$, or $\theta < \pi/2$) is necessary but not sufficient; in fact, the liquid must be more wetting than given in equation 78, i.e., the contact angle must be less than an upper bound given by:

$$1 > \cos\theta > \frac{h_G - h_L}{R} > 0, \quad \text{or} \tag{80}$$

$$0 < \theta < \arccos\frac{h_G - h_L}{R} < \pi/2. \tag{81}$$

In order to have liquid core when $Q_{GF} \gtrsim 0.71$, eq. 79 shows that the contact angle may be $< 90°$ as long as the inequality 79 is met. If, on the other hand, $Q_{GF} \lesssim 0.71$, the gas core is thinner than the liquid core for the same Q_{GF} and a gas core exists when

$$1 > \cos\theta > \frac{h_G - h_L}{R}, \quad \text{or} \tag{82}$$

$$0 < \theta < \arccos\frac{h_G - h_L}{R}. \tag{83}$$

In this case, because $\frac{h_G - h_L}{R} < 0$, it might be possible to have liquid flowing next to the wall even for "non-wetting" liquids with contact angles $\pi/2 < \theta < \arccos\frac{h_G - h_L}{R}$.

C Pressure Drop by Integral Momentum Balance with Droplet Entrainment in the Air Stream

The goal is to predict the pressure drop, Δp, given the wall shear stress, τ_W and the flow rates Q_L and Q_G, when drops of liquid break off the liquid film and are entrained in the core gas flow. Clearly this event must alter the balance between τ_W and ΔP derived in Appendix A because the liquid drops, moving at the average gas phase velocity, will carry a higher momentum than a case where all the liquid flows in the film.

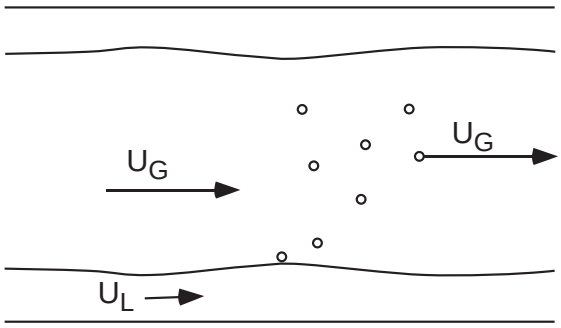

Figure 25: Schematic of annular flow with liquid drops entrained into the gas stream. The gas velocity U_G is $\gg U_L$, the liquid velocity. Once the entrained liquid drops have attained U_G in the gas stream, a fraction f_{ent} of the liquid moves with a momentum significantly higher than when that fraction was in the liquid annulus. As a result, the pressure has to reduce to compensate for the momentum needed to accelerate these drops.

We assume that

- Liquid is adjacent to the wall and air is in the core of the flow.
- Gravity is negligible.
- Some liquid droplets are entrained in the air core of the flow and no gas is entrained in the liquid film.
- The flow is incompressible, laminar, axisymmetric, fully developed, and the liquid film thickness, $t \equiv R - h$, is constant.

The liquid Q_L and gas flow Q_G rates are related to the superficial velocities by:

$$Q_L = \pi R^2 U_{LS} \tag{84}$$

$$Q_G = \pi R^2 U_{GS} \tag{85}$$

If q_{LD} is the liquid flow rate that is flowing as drops entrained in the gas phase, then conservation of liquid flow rate gives

$$Q_{LF} = Q_L - q_{LD} \tag{86}$$

If U_{LF} is the average liquid velocity in the film,

$$U_{LF} \equiv \frac{Q_{LF}}{2\pi R t}, \tag{87}$$

and substituting in eq. 86

$$U_{LF} 2\pi R t = Q_L - q_{LD} \tag{88}$$

Since $R \approx R - t$, the shear stress balance at the interface is approximately

$$\frac{\mu_L U_{LF}}{t} = \frac{\mu_G U_{GS}}{R} \tag{89}$$

Replacing U_{LF} from eq. 88 we solve for t

$$\frac{t}{R} = \left[\frac{1}{2}\frac{Q_L - q_{LD}}{Q_G}\frac{\mu_L}{\mu_G}\right]^{1/2} \tag{90}$$

To write the momentum in, we assume that the two phases are well mixed. To write the momentum out, we assume that droplets, with total flow rate q_{LD}, are convected with U_{GS} and that they do not get deposited in the liquid film. Then:

$$M|_{out} = 2\pi R h \rho_L U_{LF}^2 + \rho_G U_{GS}^2 \pi R^2 + \rho_L q_{LD} U_{GS} + P_{out}\pi R^2 \tag{91}$$

$$M|_{in} = \rho_L U_{LS}^2 \pi R^2 + \rho_G U_{GS}^2 \pi R^2 + P_{in}\pi R^2 \tag{92}$$

The change in momentum flux is balanced by the shear stress at the wall, $M|_{out} - M|_{in} = \tau_W^*$. Therefore,

$$\Delta p \equiv p_{in} - p_{out} = \frac{2\tau_W L}{R} + \frac{q_{LD}\rho_L U_{GS}}{\pi R^2} + \frac{2\rho_L t U_{LF}^2}{R} - \rho_L U_{LS}^2 \tag{93}$$

Using eqs. 88 and 90, we may write

$$t U_{LF}^2 = \left(\frac{Q_L - q_{LD}}{2\pi R}\right)^2 \frac{1}{\left(\frac{1}{2\pi}\frac{Q_L - q_{LD}}{U_{GS}}\frac{\mu_L}{\mu_G}\right)^{1/2}} = \frac{(2Q_G)^{1/2}}{4\pi^2}\frac{(Q_L - q_{LD})^{3/2}}{R^3}\left(\frac{\mu_G}{\mu_L}\right)^{1/2} \tag{94}$$

Substituting into eq. 93,

$$\Delta p = \frac{2\tau_W L}{R} + \rho_L U_{LS}^2 \left[\frac{q_{LD}\, U_{GS}}{\pi R^2 U_{LS}^2} + \left(\frac{Q_G}{2Q_L}\right)^{1/2}\left(1 - \frac{q_{LD}}{Q_L}\right)^{3/2}\left(\frac{\mu_G}{\mu_L}\right)^{1/2} - 1\right] \tag{95}$$

The only undetermined parameter in the above expression is q_{LD}. If we define the fraction of liquid drops entrained as $f_{ent} \equiv q_{LD}/Q_L$, we may write:

$$\Delta p = \frac{2\tau_W L}{R} + \rho_L U_{LS}^2 \left[f_{ent}\frac{U_{GS}}{U_{LS}} + (1 - f_{ent})^{3/2}\left(\frac{U_{GS}}{2U_{LS}}\right)^{1/2}\left(\frac{\mu_G}{\mu_L}\right)^{1/2} - 1\right] \tag{96}$$

D Flow regimes in ALS equipment operating in microgravity

We describe an estimation tool for flow regimes that might develop in two-phase flows occurring in water recovery equipment in zero gravity. The calculation is based on the flow regime map discovered by Jayawardena, Balakotaiah and Witte (1997) [1]. We have had to make reasonable assumptions about pipe diameters and flow rates for lack of concrete information in the available space systems literature (Eckart 1996 [35], Eckart 1997 [36], Wieland 1998 [37], Wieland 1998 [38], Wieland 1994 [39]). The only experiments on oxygen generation in microgravity are by Ohira *et al.*, 2001 [65] who performed experiments that used cultivated microalgae.

First we took nominal gas and liquid flow rates input into a few of the systems as shown in Eckart (1996)[35]. We assume that the gas input shown in the table refers to gas dissolved in the urine feed. We also assume that, as the pressure decreases downstream, this dissolved gas comes out of solution completely, thus generating a two-phase flow with the flow rates indicated.

We have developed an Excel worksheet that returns the flow regime and the values of the liquid and gas Reynolds numbers as the answer, for given liquid and gas mass flow rate, and pipe diameter inputs. The worksheet has fixed liquid and gas properties (density and viscosity), as well as water-air surface tension. We have assumed a surface tension value of $\sigma = 70$ dyn/cm, a good estimate for pure water but maybe as much as twice that of urine.

The liquid and gas Reynolds numbers should give a rough indication of whether the flow is laminar or turbulent. We discuss some ideas about transition mechanisms, and the usefulness of the Reynolds number to decide whether the flow is laminar.

D.1 Dimensionless Groups for Current Space ALS Hardware

In zero gravity, and because $\mu_G \ll \mu_L$ and $\rho_G \ll \rho_L$, of the seven dimensionless groups identified in section 2.1, only three independent groups remain:

$$Su \equiv \frac{\rho_L D\sigma}{\mu_L^2}, \quad Re_L \equiv \frac{U_{LS}\,\rho_L D}{\mu_L}, \quad \text{and} \quad Re_G \equiv \frac{U_{GS}\,\rho_G D}{\mu_G},$$

where $U_{GS} \equiv 4Q_G/\pi D^2$ and $U_{LS} \equiv 4Q_L/\pi D^2$ are the gas and liquid "superficial" velocities. It is clear that these are not the actual average phase velocities, but instead the velocities of the gas and liquid *if* each phase were flowing in the pipe alone.

Su is the Suratman number. It is a "Reynolds" number where the characteristic velocity is the capillary velocity scale σ/μ. For this reason, it does not involve any externally imposed velocity scale; it only depends on pipe diameter and material properties. Of course, $\{Re_G, Re_L, Su\}$ is not the only choice of groups; but it is the one that best (i.e., most compactly) correlates the data, at least in the range of

parameters probed in Jayawardena *et al.* (1997). Any other choice of groups must comprise three groups and only three.

D.2 Flow regime estimation in two-phase ALS technologies operating in Microgravity

Below is an example of a list of two-phase systems that are critical to regenerative life support technologies for water and atmosphere management. We use the flow regime maps (and regime boundaries) discussed in section 3.1.

Example: Vapor Phase Catalytic Ammonia Removal (VPCAR): From Eckart (1996, p. 224), we find $\dot{M}_L = 13$ Kg/day, $\dot{M}_G = 0.02$ Kg/day. From these, using fluid densities, we get $Q_G = 0.23$ cm^3/s and $Q_L = 0.15$ cm^3/s, $Re_G/Re_L = 7.67\ 10^{-2}$. For an assumed 1/4 inch diameter *straight cylindrical* pipe, $D = 0.64$ cm and $Su = 4.5\,10^5$. Since $Re_G/Re_L = 7.67\ 10^{-2}$ is less than $464.16\,Su^{-2/3} = 7.9\ 10^{-2}$ (the location of the left-most boundary in Fig. 2), we conclude that the flow is bubbly (although the point is so close to the boundary that one should be cautious about flow type without experimental verification). Further, since Re_G and Re_L are not large, we may surmise that both phases flow in the laminar regime. In the table below we compare three systems as found in Eckart (1996). We assume $D = 0.64$ cm, $\rho_L = 1$ g/cm^3, $\rho_G = 10^{-3}$ g/cm^3, $\mu_L = 10^{-2}$ Poise, $\mu_G = 2\ 10^{-4}$ Poise, $\sigma = 70$ dyn/cm. Note that these units are all in the CGS system so they may be entered into the dimensionless groups as is. The decision about laminar flow is based on the values of Re_G and Re_L; see more in Discussion section.

Other systems include:

Vapor Compression Distillation (VCD): From Eckart (1996, p. 221), we find $\dot{M}_L = 33$ Kg/day, $\dot{M}_G = 0.03$ Kg/day.

Thermoelectric Integrated Membrane Evaporation System (TIMES): From Eckart (1996, p. 225), we find $\dot{M}_L = 22$ Kg/day, $\dot{M}_G = 0.7$ Kg/day.

Electrolysis Plant (ELEKTRON): From Wieland (1998, p. 57, Vol. 2), we find $\dot{M}_L = 8$ Kg/day, $\dot{M}_G = 6$ Kg/day.

Supercritical Water Oxidation (SCWO): From Eckart (1996, p. 241), we find $\dot{M}_L = 25.6$ Kg/day, $\dot{M}_G = 2.59$ Kg/day.

Condensing Heat Exchanger (CHX): From Wieland (1998, p. 104, Vol. 1 and Scull *et al.* 1998), we find $\dot{M}_L = 24$ Kg/day, $\dot{M}_G = 11132$ Kg/day.

Table 1: Summary comparison of three water recovery systems for $D = 0.64$ cm. Mass flow data from Eckart (1996) and Wieland (1998)

SYSTEM	$\dot{M}_G$ Kg/day	$\dot{M}_L$ Kg/day	D cm	Re_G	Re_L	Flow Regime	Laminar?
VPCAR	0.02	13	0.64	2.3	30	Bubble	Yes
VCD	0.03	33	0.64	3.5	76	Bubble	Yes
TIMES	0.7	22	0.64	80	50	Annular	Yes
ELEKTRON	6	8	0.64	690	18	Annular	Inconclusive
SCWO	2.59	25.6	0.64	299	58	Annular	Yes
CHX	11132	24	0.64	$1.2\,10^6$	55	Annular	No

D.3 Discussion

First we address some ideas about flow regime transitions that can be gleaned from the map. For fixed Su, transition from bubble to slug happens as the ratio of superficial Reynolds numbers approaches a certain value. In our case, with a pipe diameter $D = 0.64$cm (1/4 inch), $Su = 4.5 \times 10^5$. And at transition, $U_{GS}/U_{LS} = 464.16\ Su^{-2/3} = 0.08$. When the gas superficial velocity is much less than the liquid's, we get bubble flow. In this flow, bubbles (of a certain size) at relatively low concentration (so that the gas volume fraction is $\ll 1$), move essentially at the liquid's average velocity. For fixed ratio of superficial Reynolds numbers, the transition occurs when Su exceeds a certain value. For a given material system, increasing Su is the same as increasing pipe diameter. As D increases, for fixed U_G and U_L, Reynolds number increases and we may expect inertia forces to stimulate coalescence. As enough bubbles coalesce, the bubble spans the whole pipe diameter, and a slug forms. However, a fixed ratio Re_G/Re_L may also obtain for fixed flow rates, Q_G and Q_L. If instead of U_G and U_L being fixed, the flow rates Q_G and Q_L are held fixed, an increase in D actually lowers the Reynolds number $Re = 4\,Q\,\rho/\pi\,D\,\mu$.

We believe that this case cannot be fully explained by the 2-dimensional map of Jayawardena *et al.* (1997) [1]. In principle, since the system is described by three parameters, any regime map should be sensitive to three parameters. The fact that the authors find a 2-dimensional map sufficient, may indicate that the dependence on the third parameter has been lost due to its either high or low value. Unfortunately, we do not have information on individual values of Re_G and Re_L in the map shown in Fig. 2. But we suspect that both are quite large, so that variations in a high value do not introduce additional dependencies to the map that would require the drawing of a third parametric axis. **However, one should warn users of the Jayawardena *et al.* map that, when Re_G and/or Re_L are not large, the map may not be valid. This is potentially very important for water recovery systems, where the Reynolds number for neither phase is large.**

Next, we offer some discussion on whether we can expect laminar flow. The values of Re for gas or liquid are based on each phase superficial velocity. Superficial velocities do not, in general, reflect the actual characteristic velocity of the phase in

question. Consequently, this definition of Re cannot be used to assess with certainty whether a flow is laminar or turbulent. For example, in bubbly flow, the bubbles are likely flowing at a velocity close to the liquid phase velocity; the relative phase velocity is therefore small. There is no clear guideline to assess whether a bubbly flow is laminar or turbulent.

In annular flow the situation is a bit different. According to the regime map, a condition for annular flow is $Re_G > 10\ Re_L$. Inputing typical values of fluid properties, this implies $Q_G > 10\ Q_L$. Since each phase is flowing separately in its own region of space, and typically the gas core radius $h \approx D/2$ with $(D-2h)/D \ll 1$, we may estimate more "realistic" gas and liquid velocities as: $U_G \equiv Q_G/\pi h^2$ and $U_L \equiv Q_G/\pi D(D/2-h)$. Inserting these velocities in the definition of gas and liquid Reynolds numbers, we get the following alternative definitions: $\overline{Re}_L \equiv U_L \rho_L (D/2-h)/\mu_L = Q_L\,\rho_L/\pi D = Re_L/4$ and $\overline{Re}_G \equiv U_G \rho_G D/\mu_G = Q_G\,\rho_G/\pi D + \mathrm{O}\left(\frac{D/2-h}{h}\right) = Re_G + \mathrm{O}\left(\frac{D/2-h}{h}\right)$. Although we have no criterion for the transition to turbulence in these annular flows, we may surmise that the flow should be laminar if $\overline{Re}_L$ and $\overline{Re}_G$ are obviously "too small" for turbulence.

In slug flow, assuming that the liquid slug and gas bubble move at the same velocity $U_G = U_L = U$ (i.e., there is no liquid film surrounding the gas bubble, or the film thickness $t \ll D/2$), then we may use similar arguments as those used for annular flow, but using the definition $\overline{Re}_L \equiv U \rho_L D/\mu_L$.

References

[1] S.S. Jayawardena, V. Balakotaiah, and L.C. Witte. Pattern transition maps for microgravity two-phase flows. *AICHE JOURNAL*, 43(6):1637–1640, JUN 1997.

[2] J. McQuillen. Microgravity two-phase flow . http://exploration.grc.nasa.gov/6712/2phase_flow/2phase.html.

[3] W.S. Bousman. Studies of two-phase gas-liquid flow in microgravity. CR 195434, NASA, University of Houston, FEB 1995.

[4] F.P. Chiaramonte and J.A. Joshi. Workshop on critical issues in microgravity fluids, transport, and reaction processes in advanced human support technology. TM 212940, NASA, 2004. AHST/UG Workshop, 2003.

[5] G.F. Hewitt, G. Hetsroni, G. Yadigaroglu, S. Banerjee, and M. Ishii. Short course on modelling and computation of multiphase flows. Technical report, Swiss Federal Institute of Technology (ETH), Zurich, Switzerland, MAR 2005.

[6] R.T. Lahey. Short course on transient multiphase flow and heat transfer at microgravity. Technical report, Center for Multiphase Research, RPI, Troy, NY USA 12180, SEPT 2002. NASA, Glenn Resrarch Center, Cleveland.

[7] A.E. Dukler, J.A. Fabre, J.B. Mcquillen, and R. Vernon. Gas-liquid flow at microgravity conditions - flow patterns and their transitions. *INTERNATIONAL JOURNAL OF MULTIPHASE FLOW*, 14(4):389–400, JUL-AUG 1988.

[8] J. Zhao and K. Gabriel. Two-phase flow patterns in a 90 degrees bend at microgravity. *ACTA MECHANICA SINICA*, 20:206–211, JUN 2004.

[9] T. Takamasa, T. Hazuku, N. Fukamachi, Tamura N., Hibiki T., and Ishii M. Effect of gravity on axial development of bubbly flow at low liquid reynolds number. *EXPERIMENTS IN FLUIDS*, 37(5):631–644, NOV 2004.

[10] T. Nonaka, K. Anzo, and M. Suzuki. Behaviors of interface deformation of annular liquid films and plug formation in circular pipes under microgravity. *KAGAKU KOGAKU RONBUNSHU*, 28(2):211–217, MAR 2002.

[11] B. Choi, T. Fujii, H. Asano, and K. Sugimoto. A study of the flow characteristics in air-water two-phase flow under microgravity (results of flight experiments). *JSME INTERNATIONAL JOURNAL SERIES B-FLUIDS AND THERMAL ENGINEERING*, 46(2):262–269, May 2003.

[12] J.F. Zhao, J.C. Xie, H. Lin, and W.R. Hu. Experimental study on two-phase gas-liquid flow patterns at normal and reduced gravity conditions. *SCIENCE IN CHINA SERIES E-TECHNOLOGICAL SCIENCES*, 44(5):553–560, OCT 2001.

[13] J.F. Zhao, J.C. Xie, H. Lin, W.R. Hu, A.V. Ivanov, and A.Y. Belyaev. Experimental studies on two-phase flow patterns aboard the mir space station. *INTERNATIONAL JOURNAL OF MULTIPHASE FLOW*, 27(11):1931–1944, NOV 2001.

[14] J.F. Zhao, J.C. Xie, H. Lin, W.R. Hu, A.V. Ivanov, and A.Y. Belyaev. Microgravity experiments of two-phase flow patterns aboard mir space station. *ACTA MECHANICA SINICA*, 17(2):151–159, MAY 2001.

[15] J.F. Zhao and W.R. Hu. Slug to annular flow transition of microgravity two-phase flow. *INTERNATIONAL JOURNAL OF MULTIPHASE FLOW*, 26(8):1295–1304, AUG 2000.

[16] G. Wölk, M. Dreyer, and H.J. Rath. Gas/liquid two-phase flow under low gravity conditions. *ZEITSCHRIFT FUR ANGEWANDTE MATHEMATIK UND MECHANIK*, 81(3):S577–S578, 2001.

[17] D.C. Lowe and K.S. Rezkallah. Flow regime identification in microgravity two-phase flows using void fraction signals. *INTERNATIONAL JOURNAL OF MULTIPHASE FLOW*, 25(3):433–457, APR 1999.

[18] E.K. Ungar, I.-Y. Chen, and S.H. Chan. Selection of a gravity insensitive ground test fluid and test configuration to allow simulation of two-phase flow in microgravity. In *Proceedings of the AIAA/ASME Joint Thermophysics and Heat Transfer Conference*, volume HTD-357-3, pages 37–50, New Orleans, LA, November 28-December 3, 1993, 1993.

[19] C. Colin, J. Fabre, and J. McQuillen. Bubble and slug flow at microgravity conditions: state of knowledge and open questions. *CHEMICAL ENGINEERING COMMUNICATIONS*, 141:155–173, 1996.

[20] T.R. Reinarts, F.R. Best, K.M. Miller, and W.S. Hill. Definition of two-phase flow behaviors for spacecraft design. *SPACE NUCLEAR POWER SYSTEMS*, pages 1230–1235, Jan 1991.

[21] Z.L. Wang, K.S. Gabriel, and D.L. Manz. The influences of wave height on the interfacial friction in annular gas-liquid flow under normal and microgravity conditions. *INTERNATIONAL JOURNAL OF MULTIPHASE FLOW*, 30(10):1193–1211, OCT 2004.

[22] B.J. Motil, V. Balakotaiah, and Y. Kamotani. Gas-liquid two-phase flow through packed beds in microgravity. *AICHE JOURNAL*, 49:557–565, 2003.

[23] W.S. Bousman, J.B. McQuillen, and L.C. Witte. Gas-liquid flow patterns in microgravity: Effects of tube diameter, liquid viscosity and surface tension. *INTERNATIONAL JOURNAL OF MULTIPHASE FLOW*, 22(6):1035–1053, NOV 1996.

[24] T. Takamasa, T. Iguchi, T. Hazuku, T. Hibiki, and M. Ishii. Interfacial area transport of bubbly flow under microgravity environment. *INTERNATIONAL JOURNAL OF MULTIPHASE FLOW*, 29(2):291–304, FEB 2003.

[25] A.M. Kamp, A.K. Chesters, C. Colin, and J. Fabre. Bubble coalescence in turbulent flows: A mechanistic model for turbulence-induced coalescence applied to microgravity bubbly pipe flow. *INTERNATIONAL JOURNAL OF MULTIPHASE FLOW*, 27(8):1363–1396, AUG 2001.

[26] M. Iguchi and Terauchi Y. Microgravity effects on the rising velocity of bubbles and slugs in vertical pipes of good and poor wettability. *INTERNATIONAL JOURNAL OF MULTIPHASE FLOW*, 27(2):189–2198, DEC 2001.

[27] Y. Taitel and L. Witte. The role of surface tension in microgravity slug flow. *CHEMICAL ENGINEERING SCIENCE*, 51(5):695–700, MAR 1996.

[28] C. Colin and J. Fabre. Gas-liquid pipe-flow under microgravity conditions - influence of tube diameter on flow patterns and pressure drops. *MICROGRAVITY SCIENCES: RESULTS AND ANALYSIS OF RECENT SPACEFLIGHTS ADVANCES IN SPACE RESEARCH*, 16(7):137–142, 1995.

[29] L. Zhao and K.S. Rezkallah. Pressure-drop in gas-liquid flow at microgravity conditions. *INTERNATIONAL JOURNAL OF MULTIPHASE FLOW*, 21(5):837–849, SEPT 1995.

[30] L. Zhao and K.S. Rezkallah. Gas-liquid flow patterns at microgravity conditions. *INTERNATIONAL JOURNAL OF MULTIPHASE FLOW*, 19:751–763, 1993.

[31] M.W. Wheeler, F.R. Best, and T.R. Reinarts. An investigation of two phase flow pressure drops in a reduced acceleration environment. In *AIP CONFERENCE PROCEEDINGS*, volume 271-3, pages 987–992, 1993.

[32] C. Colin. Two-phase bubbly flows in microgravity: some open questions. *MICROGRAVITY SCIENCE AND TECHNOLOGY*, 13(2):16–21, 2002.

[33] L.B. Fore, L.C. Witte, and J.B. McQuillen. Heat transfer to two-phase slug flows under reduced-gravity conditions. *INTERNATIONAL JOURNAL OF MULTIPHASE FLOW*, 23(2):301–311, APR 1997.

[34] *Modelling and Computation of Multiphase Flows Short Course Notes, Part IIB: Computational Multi-Fluid Dynamics*. Swiss Federal Institute of Technology (ETH), Zürich, Switzerland, March 14-18, 2005.

[35] P. Eckart. *Spaceflight Life Support and Biospherics*. Space Technology Library. Microcosm Press, Torrance, CA and Kluwer Academic Publishers Dordrecht, Boston, London, 1996.

[36] P. Eckart. Lunar base parametric model. *JOURNAL OF AEROSPACE ENGINEERING*, 10(2):80–90, APR 1997.

[37] P.O. Wieland. Living together in space: the design and operation of the life support systems on the international space station. TM 206956 Vol 1, NASA, 1998.

[38] P.O. Wieland. Living together in space: the design and operation of the life support systems on the international space station. TM 206956 Vol 2, NASA, 1998.

[39] P.O. Wieland. Designing for human presence in space: an introduction to environmental control and life support systems. Rp-1324, NASA, 1994.

[40] G. Kocamustafaogullari and M. Ishii. Foundation of the interfacial area transport equation and its closure relations. *Int. J. Heat and Mass Transfer*, 38:481–493, 1995.

[41] K. Hurlbert, L. Witte, F. Best, and C. Kurwitz. Scaling two-phase flows to mars and moon gravity conditions. *INTERNATIONAL JOURNAL OF MULTIPHASE FLOW*, 30:351–368, 2004.

[42] T.J. Hanratty. Workshop on scientific issues in multiphase flow - foreword. *INTERNATIONAL JOURNAL OF MULTIPHASE FLOW*, 29(7):1043–1044, JUL 2003.

[43] T.J. Hanratty, T. Theofanous, J.M. Delhaye, J. Eaton, J. McLaughlin, A. Prosperetti, S. Sundaresan, and G. Tryggvason. Workshop findings. *INTERNATIONAL JOURNAL OF MULTIPHASE FLOW*, 29(7):1047–1059, JUL 2003.

[44] T.G. Theofanous and T.J. Hanratty. Appendix 1 Report of study group on flow regimes in multifluid flow. *INTERNATIONAL JOURNAL OF MULTIPHASE FLOW*, 29(7):1061–1068, JUL 2003.

[45] S. Sundaresan, J. Eaton, D.L. Koch, and J.M. Ottino. Appendix 2 Report of study group on disperse flow. *INTERNATIONAL JOURNAL OF MULTIPHASE FLOW*, 29(7):1069–1087, JUL 2003.

[46] A. Prosperetti and G. Tryggvason. Appendix 3 Report of study group on computational physics. *INTERNATIONAL JOURNAL OF MULTIPHASE FLOW*, 29(7):1089–1099, JUL 2003.

[47] J.M. Delhaye and J.B. McLaughlin. Appendix 4 Report of study group on microphysics. *INTERNATIONAL JOURNAL OF MULTIPHASE FLOW*, 29(7):1101–1116, JUL 2003.

[48] A. Prosperetti, T.G. Theofanous, Y. Matsumoto, A. Tomiyama, and Kawaji M. Panelist comments on: Open questions and new directions in gas-liquid flows. *JOURNAL OF FLUIDS ENGINEERING-TRANSACTIONS OF THE ASME*, 126(4):508–515, JUL 2004.

[49] A. Kawahara, P.M.-Y. Chung, , and M. Kawaji. Investigation of two-phase flow pattern, void fraction and pressure drop in microchannels. *INTERNATIONAL JOURNAL OF MULTIPHASE FLOW*, 28:1411–1435, 2002.

[50] F. P. Incropera and D. P. De Witt. *Fundamentals of heat and mass transfer*. 'John Wiley & Sons, New York', 1985.

[51] M.M Awad and Y. S. Muzychka. A simple two-phase frictional multiplier calculation method. In *Proceedings of IPC 2004 International Pipeline Conference*, pages 1–9, October 4-8, 2004, Calgary, Alberta, Canada, Oct 2004.

[52] G.K. Batchelor. *An introduction to fluid dynamics*. Cambridge University Press, Cambridge, U.K., 1967.

[53] S-Y. Son and J.S. Allen. Visualization of wettability effects on microchannel two-phase flow resistance. *Transactions of the ASME*, 126:498, Aug 2004.

[54] K.A. Triplett, S.M. Ghiaasiaan, S.I. Abdel-Khalik, and D.L. Sadowski. Gas-liquid two-phase flow in microchannels. part i two-phase flow patterns. *INTERNATIONAL JOURNAL OF MULTIPHASE FLOW*, 25:377–394, 1999.

[55] L. Preziosi, K. Chen, and D.D. Joseph. Lubricted pipelining: stability of core-annular flow. *J. Fluid Mech.*, 201:323–356, 1989.

[56] G.F. Hewitt and N.S. Hall-Taylor. *Annular two-phase flows*. Pergamon Press, Oxford, 1970.

[57] A.E. Bergles, J.G. Collier, J.M. Delhaye, G.F. Hewitt, and F. Mayinger. *Two-phase flow and heat transfer in the power and process industries*. Hemisphere Publishing Corp., New York, 1981.

[58] G.F. Hewitt and A.H. Govan. Phenomenological modeling of non-equilibrium flows with phase-change. *INTERNATIONAL JOURNAL OF HEAT AND MASS TRANSFER*, 33(2):229–242, Feb 1990.

[59] K.M. Miller, E.K. Ungar, J.M. Dzenitis, and M. Wheeler. 'microgravity two-phase pressure drop data in smooth tubing'. In *Proceedings of the ASME 1993 Winter Annual Meeting,*, volume 'AMD-174/FED-175', pages 37–50, New Orleans LA, November 28-December 3, 1993, 1993.

[60] J.P. Holman. *Heat transfer*. 'McGraw Hill, New York', 1976.

[61] J.G. Knudsen and D.L. Katz. *Fluid dynamics and heat transfer*. McGraw Hill, New York, 1958.

[62] M.S. Chitti and N.K. Anand. An analytical model for local heat transfer coefficients for forced convective condensation inside smooth horizantal tubes. *Int. J. Heat and Mass Transfer*, 38(4):615–672, 1995.

[63] G.T. Elicson. Dynamic Benchmarking of Tremolo- A Program for Pipeline Two-Phase Flow Transient Analysis. Paper number 195434, 9th International Topical Meeting on Nuclear Reactor Thermal Hydraulics (NURETH-9), San Francisco, California, 1999.

[64] A. Ghajar. Two Phase Heat Transfer in Gas-Liquid Non-Boiling Pipe Flows. Paper number K2, 3rd International Conference on Heat Transfer, HEFAT2004, Cape Town, S. Africa, 2004.

[65] Y. Ohira, Y. Kuga, K. Idogawa, T. Fukuda, and Ando K. Formation map of air-liquid hollow profile under microgravity. *JOURNAL OF CHEMICAL ENGINEERING OF JAPAN*, 33(3):336–341, APR 2000.

REPORT DOCUMENTATION PAGE

Form Approved
OMB No. 0704-0188

1. AGENCY USE ONLY (*Leave blank*)	2. REPORT DATE	3. REPORT TYPE AND DATES COVERED
	January 2006	Final Contractor Report

4. TITLE AND SUBTITLE

Two Phase Flow Modeling: Summary of Flow Regimes and Pressure Drop Correlations in Reduced and Partial Gravity

5. FUNDING NUMBERS

WBS–22–101–53–01
NCC3–975

6. AUTHOR(S)

R. Balasubramaniam, E. Ramé, J. Kizito, and M. Kassemi

7. PERFORMING ORGANIZATION NAME(S) AND ADDRESS(ES)

National Center for Space Exploration Research
Glenn Research Center
21000 Brookpark Road
Cleveland, Ohio 44135

8. PERFORMING ORGANIZATION REPORT NUMBER

E–15422

9. SPONSORING/MONITORING AGENCY NAME(S) AND ADDRESS(ES)

National Aeronautics and Space Administration
Washington, DC 20546–0001

10. SPONSORING/MONITORING AGENCY REPORT NUMBER

NASA CR—2006-214085

11. SUPPLEMENTARY NOTES

Project Manger, Brian Quigley, Exploration Systems Division, NASA Glenn Research Center, organization code PTO, 216–433–8672.

12a. DISTRIBUTION/AVAILABILITY STATEMENT

Unclassified - Unlimited
Subject Category: 34

Available electronically at http://gltrs.grc.nasa.gov

This publication is available from the NASA Center for AeroSpace Information, 301–621–0390.

12b. DISTRIBUTION CODE

13. ABSTRACT ***(Maximum 200 words)***

The purpose of this report is to provide a summary of state-of-the-art predictions for two-phase flows relevant to Advanced Life Support. We strive to pick out the most used and accepted models for pressure drop and flow regime predictions. The main focus is to identify gaps in predictive capabilities in partial gravity for Lunar and Martian applications. Following a summary of flow regimes and pressure drop correlations for terrestrial and zero gravity, we analyze the fully developed annular gas-liquid flow in a straight cylindrical tube. This flow is amenable to analytical closed form solutions for the flow field and heat transfer. These solutions, valid for partial gravity as well, may be used as baselines and guides to compare experimental measurements. The flow regimes likely to be encountered in the water recovery equipment currently under consideration for space applications are provided in an appendix.

14. SUBJECT TERMS	15. NUMBER OF PAGES
Fluid dynamics	72
	16. PRICE CODE

17. SECURITY CLASSIFICATION OF REPORT	18. SECURITY CLASSIFICATION OF THIS PAGE	19. SECURITY CLASSIFICATION OF ABSTRACT	20. LIMITATION OF ABSTRACT
Unclassified	Unclassified	Unclassified	